NASA Technical Memorandum 84645

Interference Effects of Aft Reaction-Control Yaw Jets on the Aerodynamic Characteristics of a Space Shuttle Orbiter Model at Supersonic Speeds

Peter F. Covell
Langley Research Center
Hampton, Virginia

ıtional Aeronautics
and Space Administration

Scientific and Technical Information Branch

1983

SUMMARY

An experimental wind-tunnel investigation has been conducted to determine the interference effects of aft reaction-control-system (RCS) yaw jet plumes on a 0.0125-scale Space Shuttle orbiter model. The tests were conducted in the Langley Unitary Plan Wind Tunnel at free-stream Mach numbers of 2.50, 3.50, and 4.50 and at a Reynolds number per foot of 3.74×10^6. Values of jet-to-free-stream mass-flow ratio corresponding to design reentry flight levels as well as higher off-design values were tested. Other test variables included the number and position of operating jets, model angle of attack, and model angle of sideslip.

The reaction-control jet plume creates a flow blockage above and behind the wing on the side in which the jet exhausts. Flow separations result on the wing upper surface and fuselage side and cause positive pitching-moment and side-force increments and negative yawing-moment and rolling-moment increments for left-side firing jets. These effects occur primarily at angles of attack above 10° and decrease slightly as Mach number increases. The yawing-moment interference increments are favorable and result in a maximum jet thrust amplification of 10 to 20 percent. As sideslip angle varies from positive to negative, the jet interference effects are delayed to a higher angle of attack. As a result of this investigation, the aft RCS was certified for operation at supersonic Mach numbers prior to the first flight of the space transportation system (STS-1).

INTRODUCTION

The National Aeronautics and Space Administration has conducted extensive wind-tunnel studies on models of the Space Shuttle orbiter. The results of these studies are compiled in reference 1. One study was undertaken to determine the jet plume interference effects of the reaction control system (RCS) during atmospheric flight (ref. 2). The RCS was originally designed to augment the aerodynamic controls for reentry and launch abort conditions above Mach 6. However, further analyses indicated the need for aft RCS yaw jet operation between Mach 6 and Mach 1, at which point the aerodynamic controls attain sufficient effectiveness to provide full vehicle control. Therefore, further studies were required to certify the RCS for operation at supersonic speeds prior to the first flight of the space transportation system (STS-1).

The purpose of the present investigation was to determine the interference effects of aft RCS yaw jet plumes on a 0.0125-scale orbiter model at supersonic speeds. High-pressure gaseous nitrogen was used for the jet plume simulation. The tests were conducted in the Langley Unitary Plan Wind Tunnel at free-stream Mach numbers of 2.50, 3.50, and 4.50, and a Reynolds number per foot of 3.74×10^6. Reaction-control jet-to-free-stream mass-flow ratios corresponding to design reentry flight levels as well as several higher off-design values were tested. Other test variables included the number and position of jets firing, model angle of attack, and model angle of sideslip.

SYMBOLS

The aerodynamic coefficient data are referenced to the body axis system. The moment reference was located at 65 percent of the body length aft of the nose. Thrust-removed aerodynamic coefficients are presented unless otherwise stated.

A_t jet nozzle throat area, 0.001176 in^2

b reference span, 11.708 in.

C_d discharge coefficient, $\frac{\text{Actual mass-flow rate}}{\text{Ideal mass-flow rate}}$

C_l rolling-moment coefficient, $\frac{\text{Rolling moment}}{qSb}$

C_m pitching-moment coefficient, $\frac{\text{Pitching moment}}{qS\bar{c}}$

C_N normal-force coefficient, $\frac{\text{Normal force}}{qS}$

C_n yawing-moment coefficient, $\frac{\text{Yawing moment}}{qSb}$

C_Y side-force coefficient, $\frac{\text{Side force}}{qS}$

$\bar{c}$ wing mean geometric chord, 5.935 in.

M free-stream Mach number

p static pressure, psi

$p_{t,j}$ jet total pressure, psi

q free-stream dynamic pressure, psi

R gas constant, ft-lbf/°R lbm

S reference area, 60.525 in^2

T_t total temperature, °R

W mass-flow rate, lbm/sec

Y side force, lbf

α angle of attack, deg

β angle of sideslip, deg

γ ratio of specific heats

Δ difference between jet-on and jet-off coefficients

δ_a aileron deflection, deg

δ_e elevon deflection, deg

θ_n nozzle divergence angle, deg

Subscripts:

bal balance

j jet

N_2 nitrogen

∞ free-stream conditions

Abbreviations:

OMS orbital maneuvering system

RCS reaction control system

STA station

APPARATUS AND TESTS

Model

A 0.0125-scale Space Shuttle orbiter model with integral reaction-control jet nozzles was employed in the wind-tunnel tests. The model dimensions are shown in figure 1. The elevons, body flap, and rudder were set at 0°, and the speedbrake was set at 55° for these tests. A photograph of the model installed in the test section is shown as figure 2. High-pressure gaseous nitrogen was used as the jet simulation medium. A hollow sting and flow-through balance were used to supply the nitrogen to a plenum in the model nose section. Internal passages from the nose plenum to an aft plenum provided for aft RCS jet operation. The desired jet firing configuration was obtained by plugging the unused nozzles. Only the aft reaction-control yaw jets located on the left OMS pod were employed for these tests.

Measurement Techniques

A five-component, flow-through strain-gage balance built specifically for these tests was used to measure the combined aerodynamic and reaction-control jet thrust forces and moments on the model. The balance did not contain the axial-force-measuring component. The jet supply pressure was measured by means of a total-pressure probe located at the connection between the sting and the nitrogen supply line. A thermocouple located further upstream in the nitrogen supply line measured the total temperature of the nitrogen. These measurements were used in calculating the jet mass-flow rate as outlined in the Data Reduction section. A backup measurement of the jet mass-flow rate was provided by a turbine flowmeter.

Qualitative analyses of the flow field were performed using the schlieren, oil flow, and vapor screen flow visualization techniques. References 3 and 4 contain descriptions of these techniques.

Data Reduction

The combined aerodynamic forces and moments, which include the RCS jet interference effects, were computed as follows (side-force component used as an example):

$$Y = Y_{bal} - k_{T,Y}p_{t,j} - k_{p,Y}p_{t,j} \tag{1}$$

where $k_{T,Y}$ is the balance RCS jet thrust constant, $k_{p,Y}$ is the balance internal pressure tare constant (both in lbf/psi), and $p_{t,j}$ is the jet total pressure (psi). The balance term Y_{bal} includes the combined aerodynamic effect (plus jet interference), the jet thrust, and the balance internal pressure tares. The $k_{T,Y}p_{t,j}$ term in equation (1) corrects the balance term for the jet thrust effect. Static-thrust calibrations were performed at an ambient pressure of about 1.2 psi with the wing removed to eliminate possible jet impingement effects. These static-thrust calibrations were within 2 percent of those obtained at near vacuum static conditions (p_∞ = 0.024 psi) in the Rockwell Rocket Nozzle Test Facility. Hence, effects of static-pressure variation on the jet thrust were considered negligible for the wind-tunnel conditions tested (p_∞ varied from 0.2 to 1.2 psi). Note that only the side force, yawing moment, and rolling moment required jet thrust corrections. The $k_{p,Y}p_{t,j}$ term in equation (1) corrects the balance term for tares due to the high balance internal pressures.

The mass-flow rate for each operating RCS nozzle was computed using the following equation, which is a modification of equation (4.17) in reference 5, page 85:

$$W_j = \sqrt{\left(\frac{\gamma_{N_2}}{R_{N_2}}\right)\left(\frac{2}{\gamma_{N_2}+1}\right)^{\frac{\gamma_{N_2}+1}{\gamma_{N_2}-1}}} \frac{p_{t,j}}{\sqrt{T_{t,j}}} A_t C_d = 0.5229 \frac{p_{t,j}}{\sqrt{T_{t,j}}} A_t C_d \tag{2}$$

The jet total pressure was determined from the nitrogen supply pressure corrected for internal pressure losses between the probe and the RCS jet plenum. The values for the discharge coefficient were provided from previous unpublished Rockwell calibrations.

The mass-flow ratio is defined as the ratio of the RCS jet mass-flow rate to a reference free-stream mass-flow rate. The reference free-stream mass-flow rate was computed using the following equation (ref. 5, page 82):

$$W_\infty = \left(\sqrt{\frac{\gamma_{air}}{R_{air}}}\right)\left(\frac{p_\infty}{\sqrt{T_{t,\infty}}} M\right)\sqrt{1 + \frac{\gamma_{air}-1}{2} M^2}\, S = 0.9188 \frac{p_\infty}{\sqrt{T_{t,\infty}}} M\sqrt{1 + 0.2M^2}\, S \tag{3}$$

The mass-flow ratio for each RCS nozzle is:

$$\frac{W_j}{W_\infty} = 0.5691 \frac{p_{t,j}}{p_\infty} \sqrt{\frac{T_{t,\infty}}{T_{t,j}}} \frac{1}{M\sqrt{1 + 0.2M^2}} \frac{A_t}{S} C_d \qquad (4)$$

Note that this mass-flow-ratio definition differs from the mass-flow parameter defined in reference 2 by a trigonometric function of the nozzle divergence angle ($\sin \theta_n$). The mass-flow ratio for configurations in which there is more than one RCS nozzle operating is the sum of the individual nozzle mass-flow ratios divided by the number of nozzles.

Test Conditions

The tests were conducted in the high Mach number test section of the Langley Unitary Plan Wind Tunnel at Mach numbers of 2.50, 3.50, and 4.50 and at a Reynolds number per foot of 3.74×10^6. A detailed description and calibration of this facility are contained in reference 4. A stagnation temperature of 585°R was maintained for Mach numbers of 2.50 and 3.50, and a stagnation temperature of 610°R was maintained for a Mach number of 4.50. The tunnel air dew point was maintained sufficiently low to assure negligible condensation effects in the test section.

Model angles of attack were varied from -4° to 26°, and angles of sideslip were varied from -2° to 2°. Boundary-layer transition on the model surface was induced by individually spaced No. 25 (0.03 in.) grit located 0.4 in. aft of the wing and vertical-tail leading edge and 1.2 in. aft of the nose. See reference 6 for a detailed description of grit-induced boundary-layer transition characteristics.

The reaction-control jet operating conditions were based on the mass-flow ratio, which was varied from 0 (jet off) to 0.0072. Corresponding jet pressure ratios ($p_{t,j}/p_\infty$) varied from jet off to 6200. The jet total temperature was maintained between 500°R and 540°R.

RESULTS AND DISCUSSION

The longitudinal aerodynamic characteristics of the orbiter with three operating RCS yaw jets on the left OMS pod are presented in figure 3. The effect of the jet plume interference is to slightly increase the pitching-moment coefficient at the higher angles of attack ($\alpha > 10°$). The onset of this jet plume interference effect on C_m occurs at decreasing angles of attack as the jet mass-flow ratio increases. Only small elevon deflections ($\delta_e < 3°$, ref. 1) are required to null this C_m interference increment. Interference effects on normal-force coefficient are insignificant.

The lateral-directional aerodynamic characteristics for three operating RCS yaw jets are shown in figure 4. In general, the jet plume induces negative yawing-moment and positive side-force coefficients at all angles of attack. The magnitude of the jet interference effects increases with increasing mass-flow ratio. At higher angles of attack ($\alpha > 10°$), negative jet-plume-induced rolling-moment coefficients occur, while slightly positive values are induced at low angles. As Mach number increases, the magnitude of the maximum jet plume interference effects for a given mass-flow

ratio and constant angle of attack decreases slightly. The angles of attack at which a sharp increase in the magnitude of C_Y, C_n, and C_l occurs coincide approximately with the onset of the C_m interference. Note that the jet-off data do not fall on the zero coefficient axes. This condition is most likely due to model asymmetry.

An indication of how the RCS jet plume induces the above-mentioned interference effects can be determined from various flow visualization methods. Oil flow pictures (fig. 5) show that the jet-off flow separation, which occurs on the wing upper surface at an angle of attack of 20°, is further aggravated by the presence of the jet plume located behind and above the left wing. The jet plume tends to act as a flow blockage above and behind the wing. This blockage moves the flow separation region further upstream. This larger flow separation region, with associated higher than unseparated surface pressures, most likely results in the negative C_l noted in figure 4. Since this flow separation region is primarily located behind the moment center, a positive C_m increment can occur. This jet plume flow blockage also appears to induce flow separations on the OMS pod and aft fuselage side, with associated increased surface pressures, which probably result in the positive values of C_Y and negative values of C_n noted in figure 4. Vapor screen photographs (fig. 6) with the light plane located at about the foremost jet orifice also indicate the extent to which the jet plume affects the flow above the wing. Notice that only small disturbances occur at $W_j/W_\infty = 0.0005$ (maximum design reentry condition for the test Mach numbers), while the region affected at $W_j/W_\infty = 0.0024$ is quite extensive. Schlieren photographs (fig. 7) show the jet penetration into the flow. The jet plume itself does not appear to expand far enough upstream to impinge upon the elevon (even though the elevon was removed for these pictures); hence, the interference effects observed previously most likely are due to plume-induced flow disturbances only.

Presented in figure 8 are the incremental jet plume interference effects on lateral-directional aerodynamic characteristics (for example, $\Delta C_l = C_l(\text{jet on}) - C_l(\text{jet off})$) at the angles of attack corresponding to the Shuttle reentry profile (see ref. 1). The interference effects for the mass-flow ratio corresponding to design reentry conditions, $W_j/W_\infty \leq 0.0005$, are negligible. At higher values of mass-flow ratio corresponding to off-design conditions such as would occur at higher altitudes, the interference effects on C_l are easily controlled by aileron deflections ($\delta_a < 1.5°$, ref. 1). The C_n interference increments are in the favorable direction and result in a slight amplification of the jet thrust yawing moment.

The effect of angle of sideslip on the incremental lateral-directional aerodynamic characteristics for three operating jets is shown in figure 9. In general the onset of the jet plume interference is delayed to a higher angle of attack as the angle of sideslip varies from positive to negative at the higher mass-flow ratios. This delay is due to the fact that the jet plume is less effective in disturbing a windward side, wing-body flow field than a leeward side, wing-body flow field.

By reducing the number of operating jets from three to one, the magnitude of the RCS jet plume interference effects is decreased as expected, and their onset is delayed to a higher angle of attack (see fig. 10). Varying the location of the single operating jet caused only negligible differences in the jet plume effects.

Shown in figure 11 are the values of the yawing-moment coefficient due to jet thrust ($C_{n,j}$) and jet plume interference (ΔC_n) for three operating jets. In general, a 10- to 20-percent (maximum) amplification of $C_{n,j}$ occurs at higher angles of

attack ($\alpha > 10°$) due to tne jet plume interference. At lower angles of attack ($\alpha < 5°$) a 3- to 7-percent amplification of $C_{n,j}$ results.

CONCLUSIONS

A wind-tunnel investigation has been conducted to determine the interference effects of aft reaction-control-system (RCS) yaw jet plumes on a 0.0125-scale Space Shuttle orbiter model. Three left-side yaw jet combinations were tested at free-stream Mach numbers of 2.50, 3.50, and 4.50 with a Reynolds number per foot of 3.74×10^6. Values of jet-to-free-stream mass-flow ratio corresponding to design reentry flight levels as well as several higher off-design values were tested. As a result of this study, the aft RCS was certified for operation at supersonic Mach numbers prior to the first flight of the space transportation system (STS-1).

The results of this investigation indicate the following conclusions:

1. The jet plume creates a blockage above and behind the wing on the side in which the jet exhausts. Flow separations occur on the wing upper surface and fuselage side and result in positive pitching-moment and side-force interference effects, and negative yawing-moment and rolling-moment interference effects for left-side firing jets. These effects occur primarily at angles of attack greater than 10°.

2. As Mach number increases, the magnitude of the jet interference effects on the lateral-directional coefficients decreases slightly for constant mass-flow ratio and angle of attack.

3. The onset of the jet plume interference effects occurs at a lower angle of attack as mass-flow ratio increases.

4. The yawing-moment interference increment is favorable and results in a maximum jet thrust amplification of 10 to 20 percent.

5. As sideslip angle varies from positive to negative, the onset of jet plume interference effects is delayed to a higher angle of attack.

6. The onset of the jet plume interference is delayed to a higher angle of attack when the number of jets operating is reduced from three to one.

7. At maximum design reentry conditions, which correspond to the lowest mass-flow ratio tested (0.0005), the jet plume interference effects are very small.

Langley Research Center
National Aeronautics and Space Administration
Hampton, VA 23665
April 14, 1983

REFERENCES

1. Aerodynamic Design Data Book. Volume I: Orbiter Vehicle. NASA CR-160386, 1978.

2. Rausch, J. R.: Space Shuttle Orbiter Rear Mounted Reaction Control System Jet Interaction Study. Rep. No. CASD-NSC-77-003 (Contract NAS9-14095), Convair Div., General Dynamics, May 1977. (Available as NASA CR-151487.)

3. Hunter, William W., Jr.; and Foughner, Jerome T., Jr., eds.: Flow Visualization and Laser Velocimetry for Wind Tunnels. NASA CP-2243, 1982.

4. Jackson, Charlie M., Jr.; Corlett, William A.; and Monta, William J.: Description and Calibration of the Langley Unitary Plan Wind Tunnel. NASA TP-1905, 1981.

5. Shapiro, Ascher H.: The Dynamics and Thermodynamics of Compressible Fluid Flow. Volume I. Ronald Press Co., c.1953.

6. Stallings, Robert L., Jr.; and Lamb, Milton: Effects of Roughness Size on the Position of Boundary-Layer Transition and on the Aerodynamic Characteristics of a 55° Swept Delta Wing at Supersonic Speeds. NASA TP-1027, 1977.

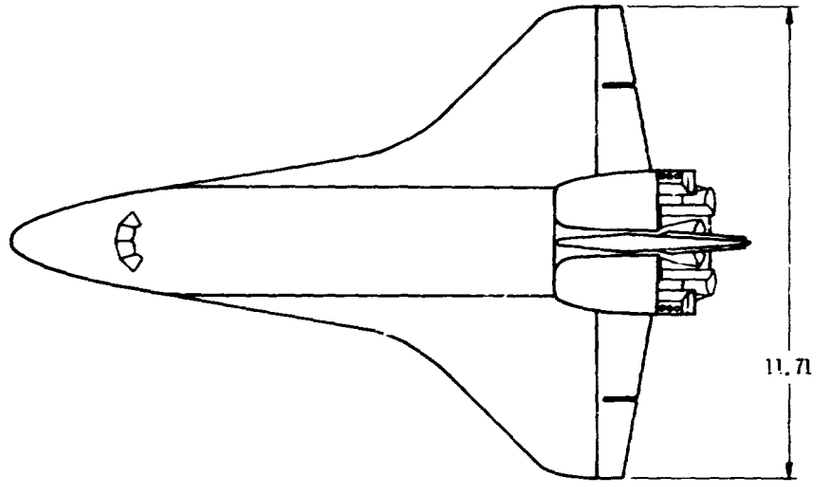

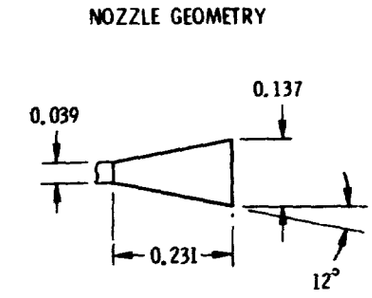

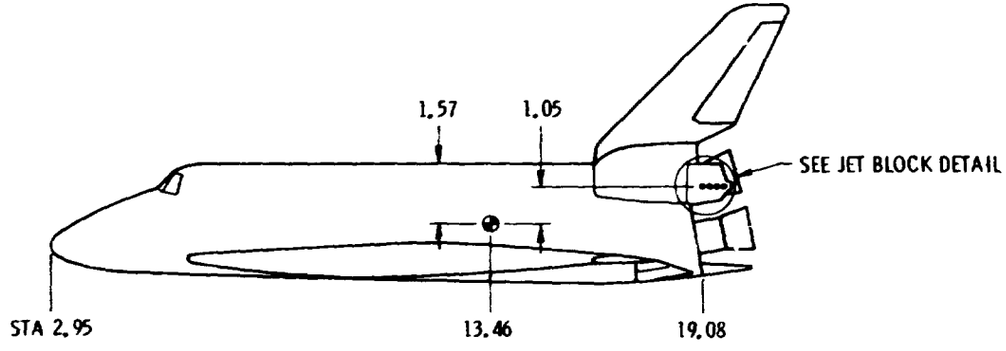

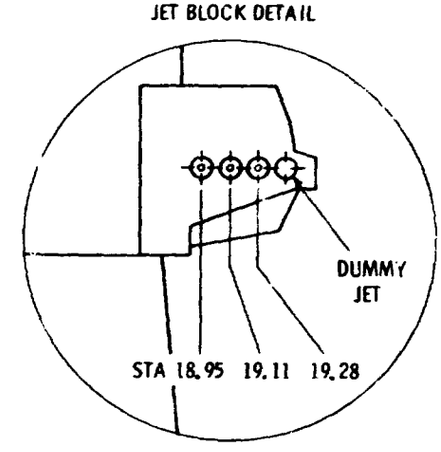

Figure 1.- Sketch of model detail. All dimensions are in inches.

ORIGINAL PAGE IS
OF POOR QUALITY

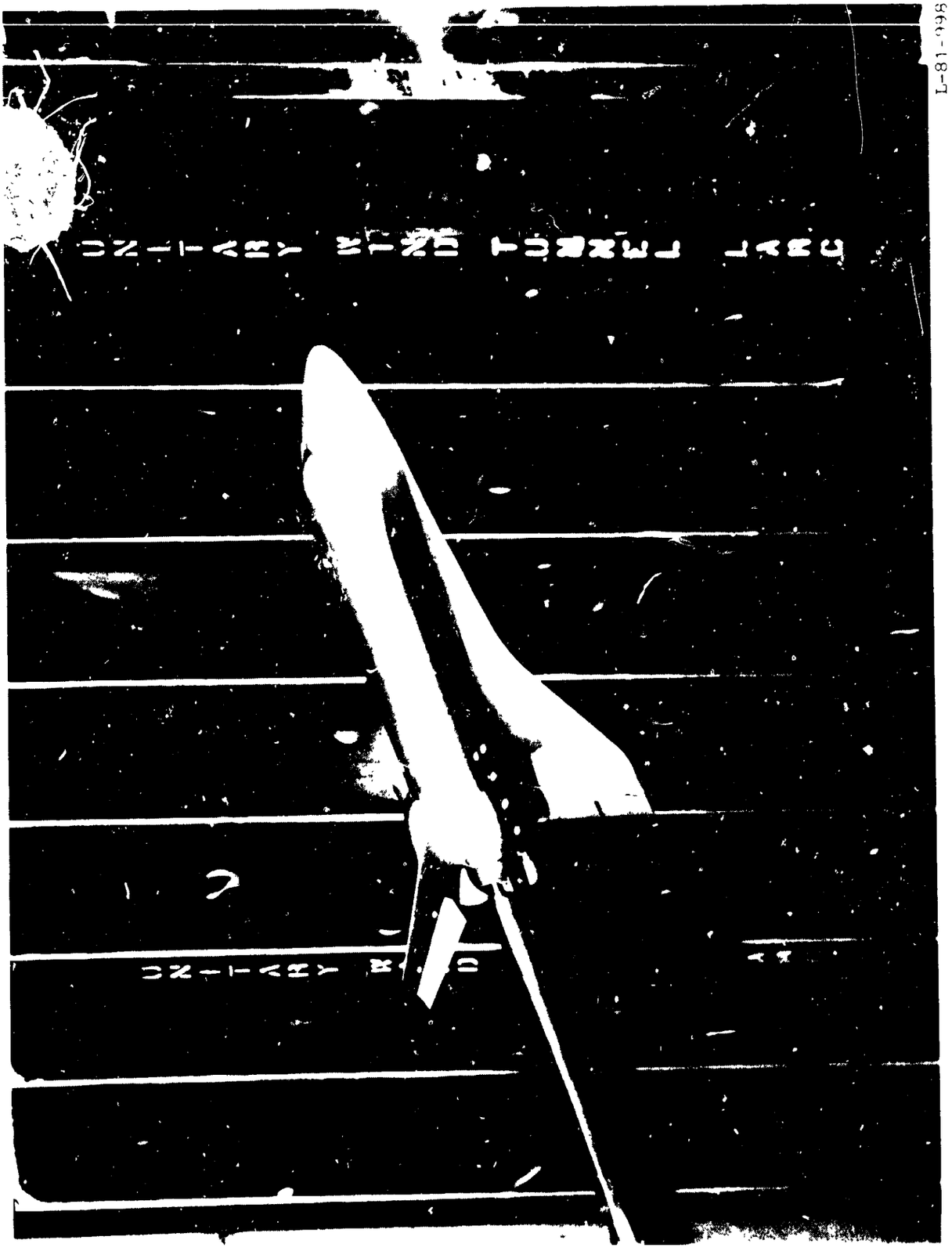

L-81-998

Figure 2.- Model in wind tunnel.

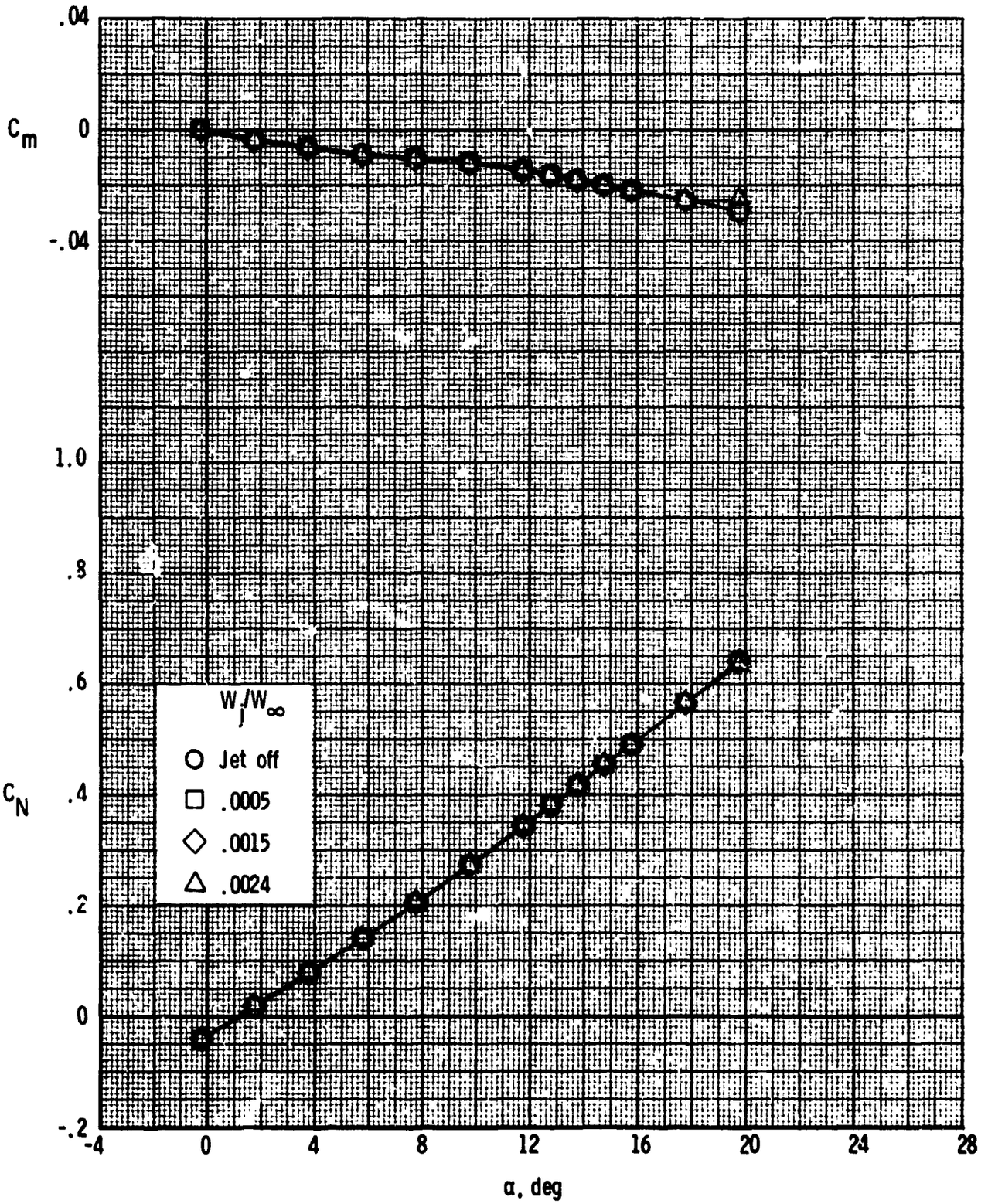

(a) M = 2.50.

Figure 3.- Effect of jet mass-flow ratio on longitudinal aerodynamic characteristics. Three yaw jets firing.

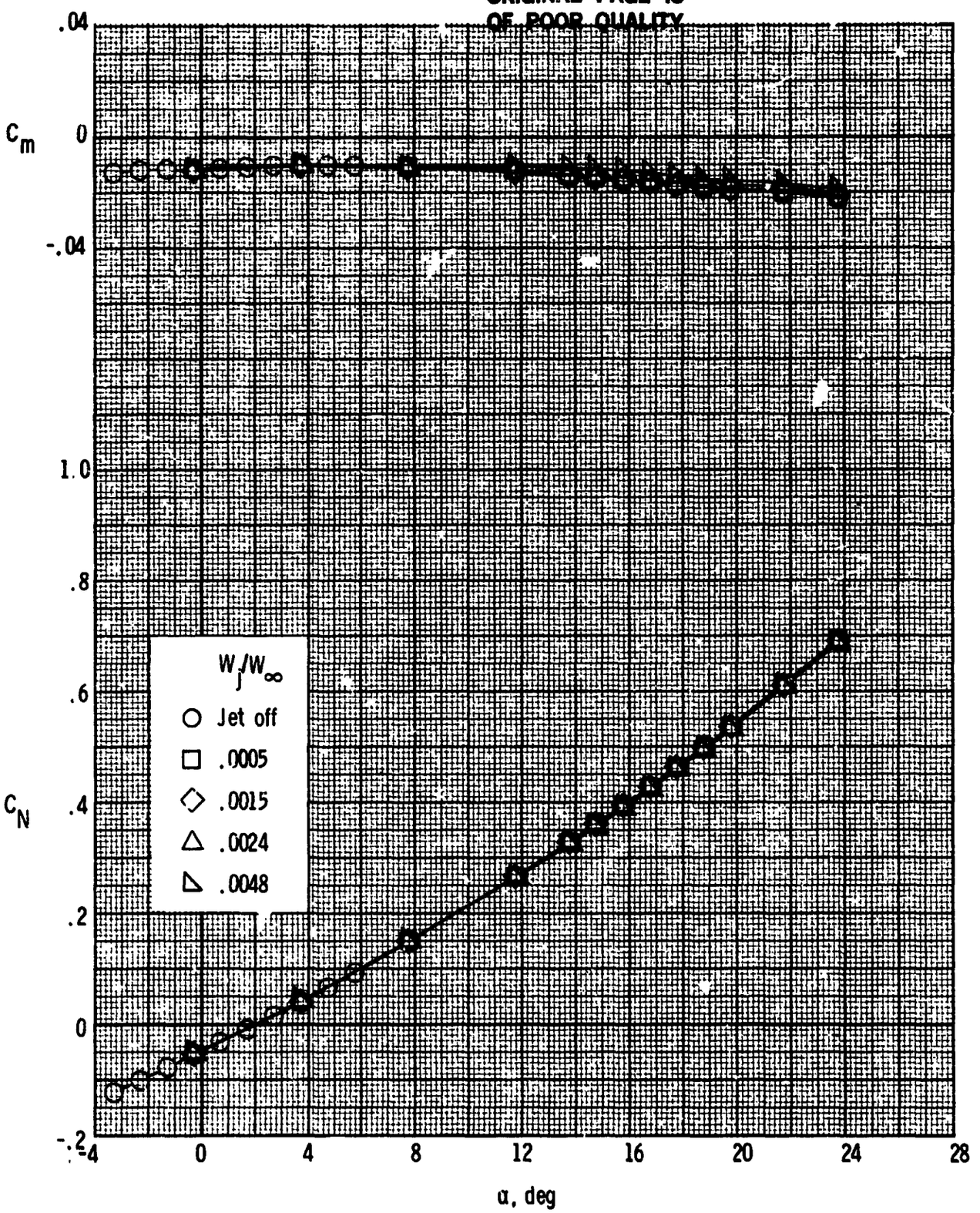

(b) M = 3.50.

Figure 3.- Continued.

ORIGINAL PAGE IS
OF POOR QUALITY

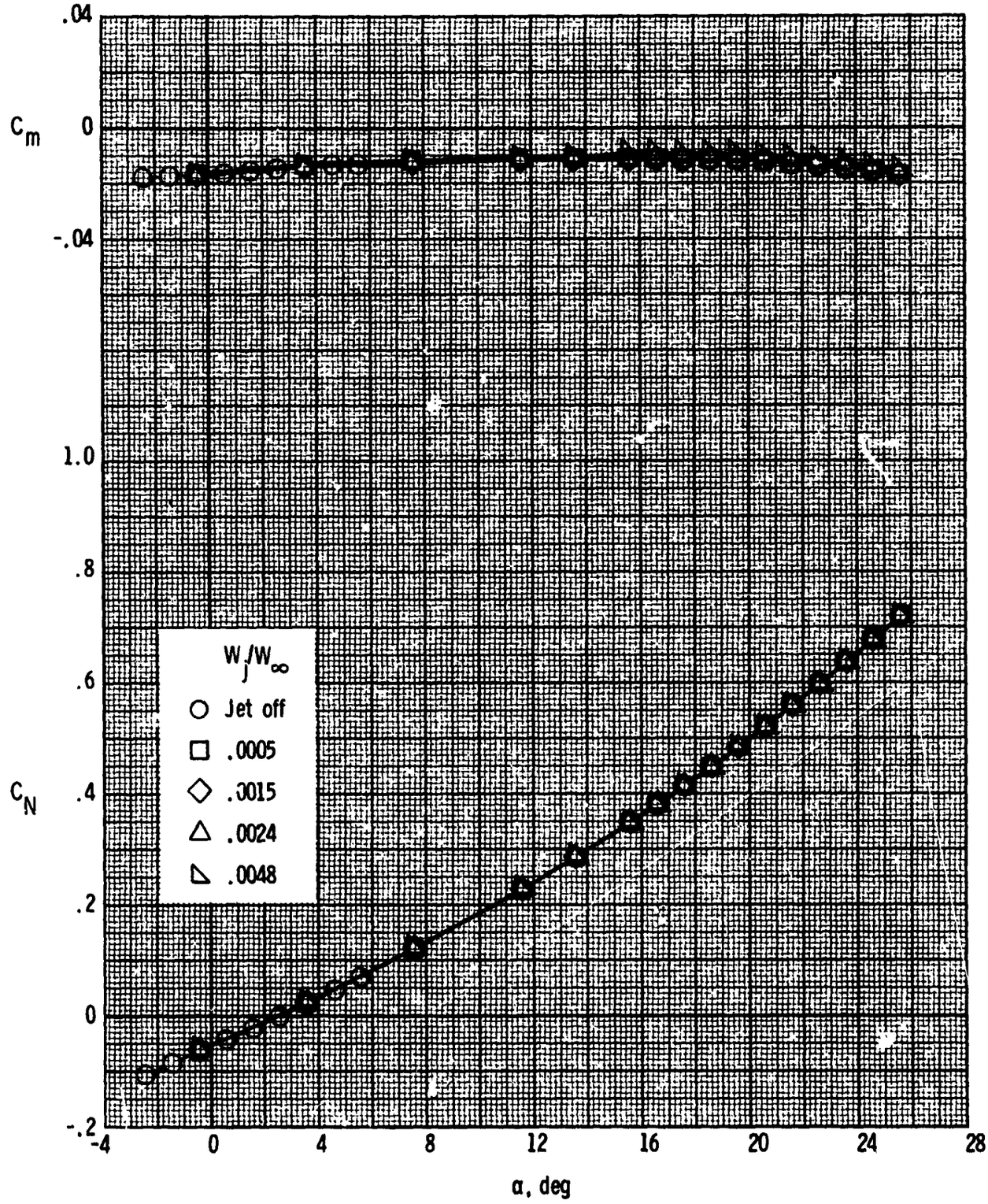

(c) M = 4.50.

Figure 3.- Concluded.

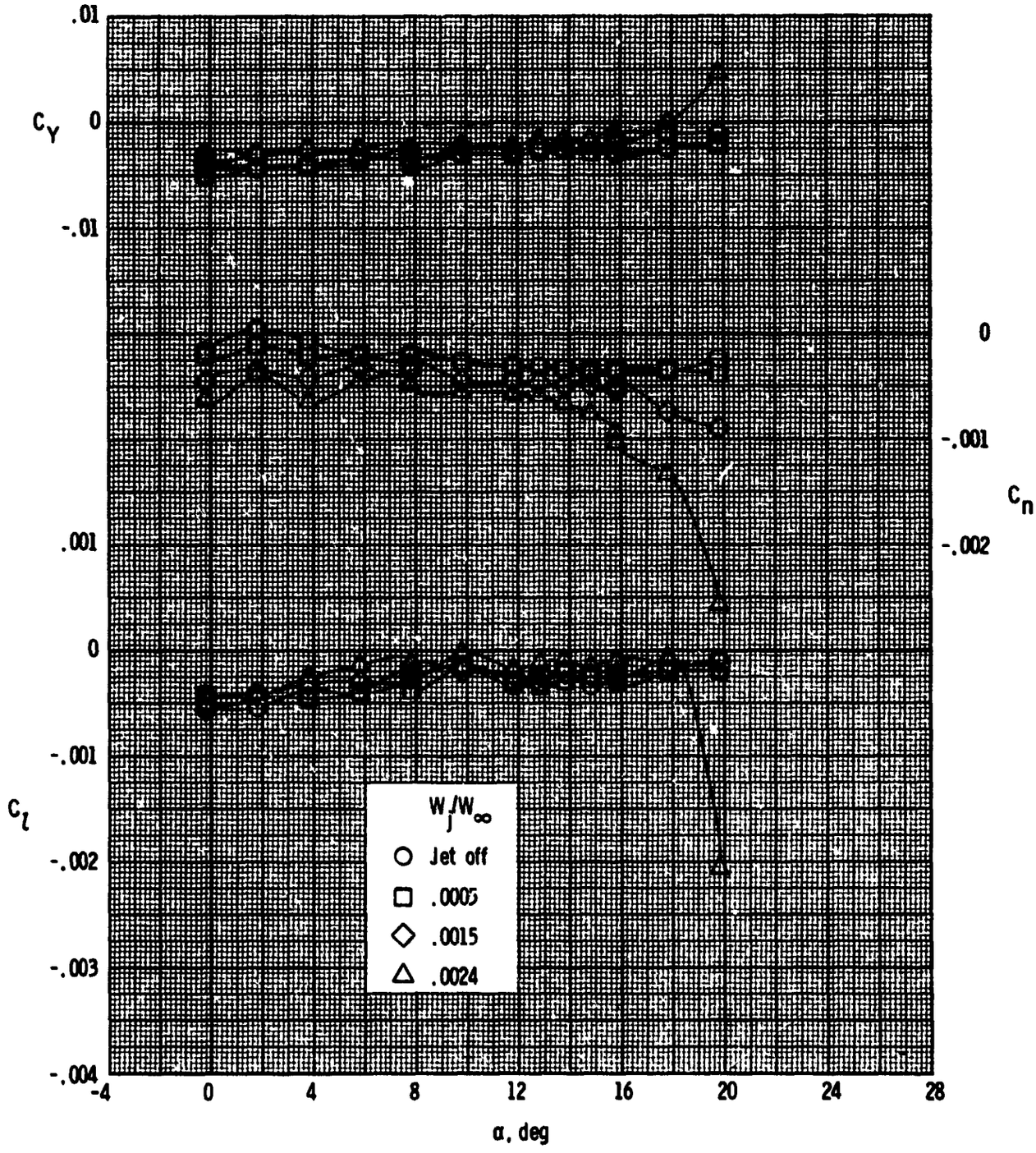

(a) M = 2.50.

Figure 4.- Effect of jet mass-flow ratio on lateral-directional aerodynamic characteristics. Three yaw jets firing.

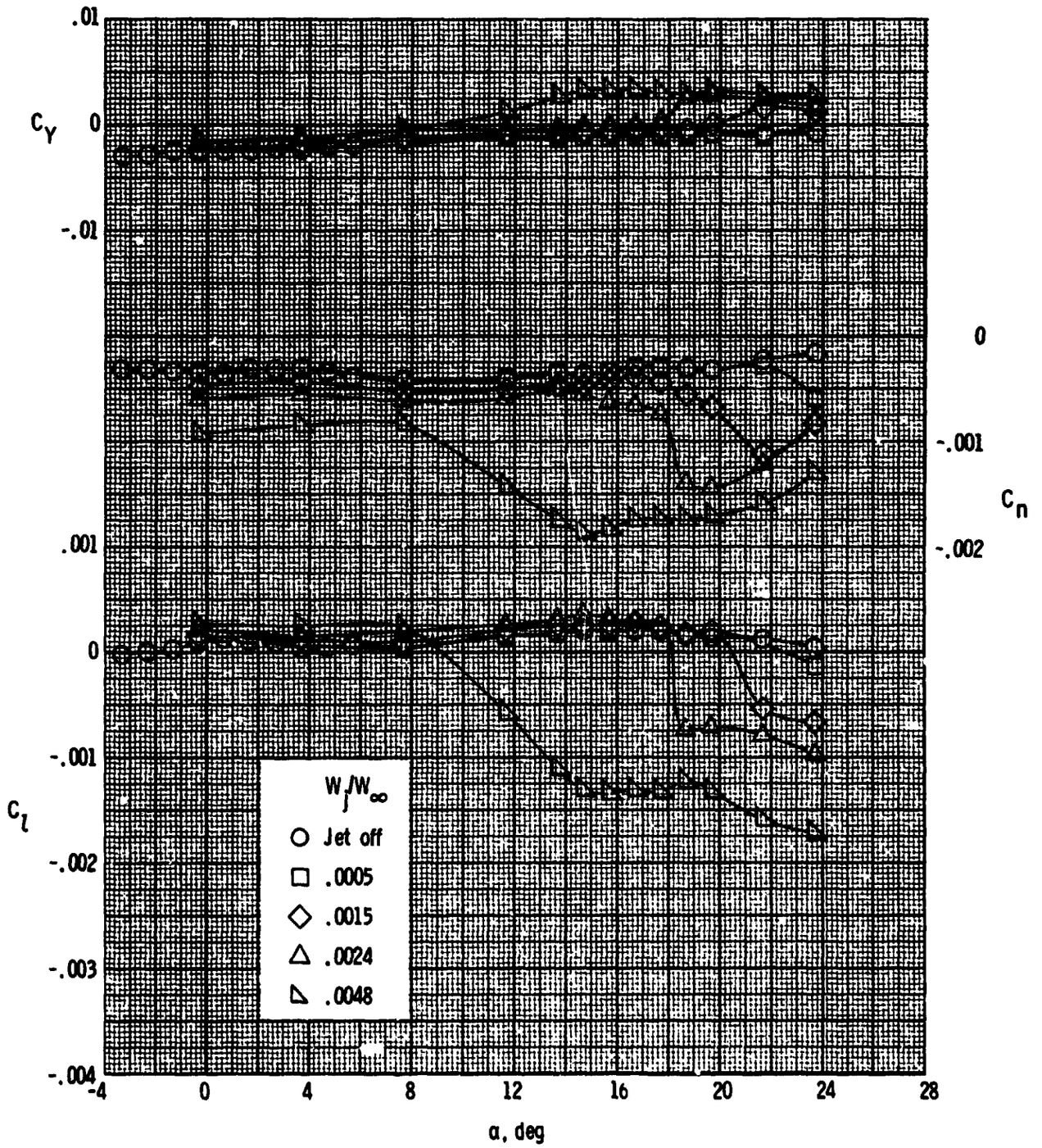

(b) M = 3.50.

Figure 4.- Continued.

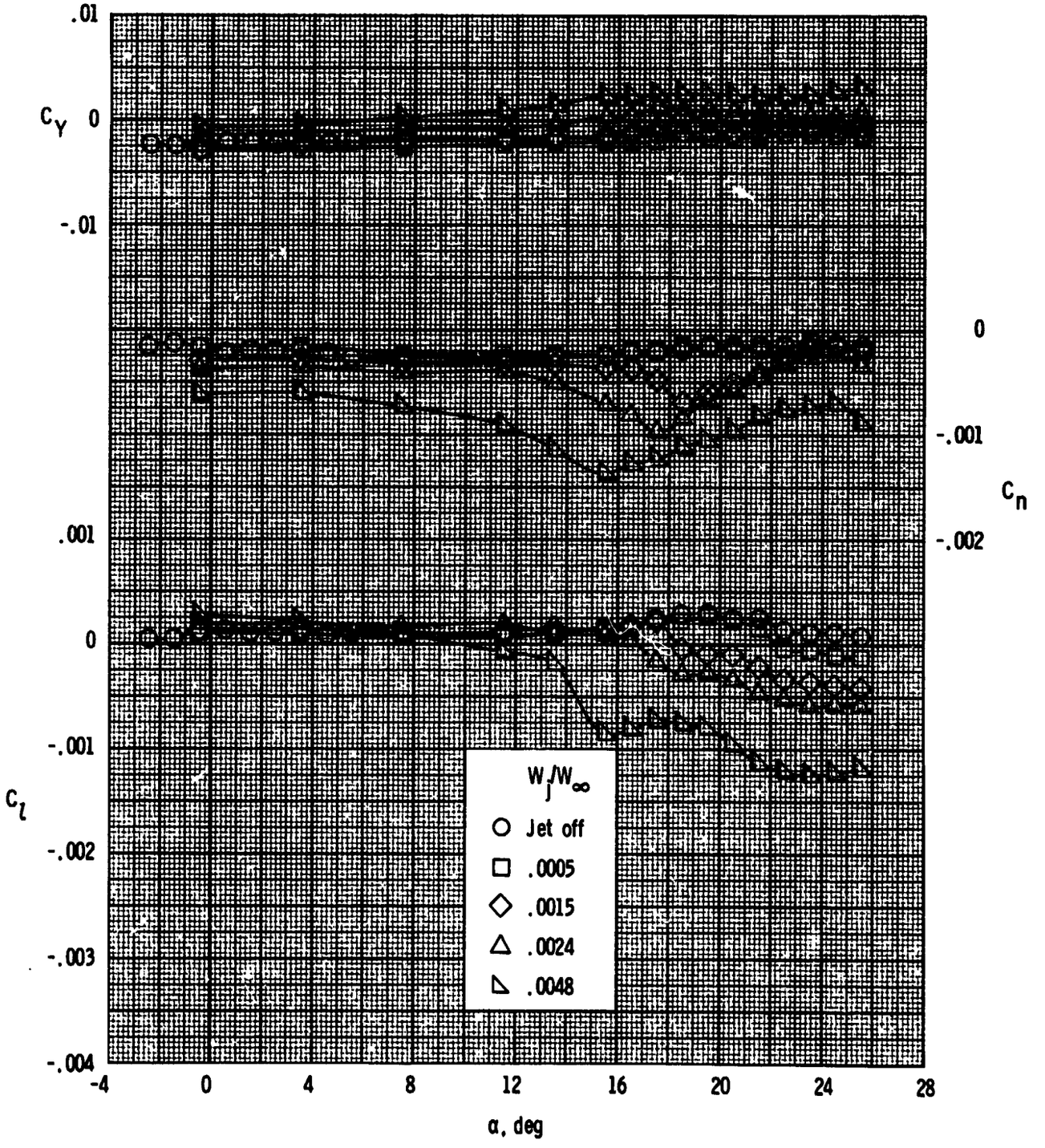

(c) M = 4.50.

Figure 4.- Concluded.

Jet off

$W_j/W_\infty = 0.0024$

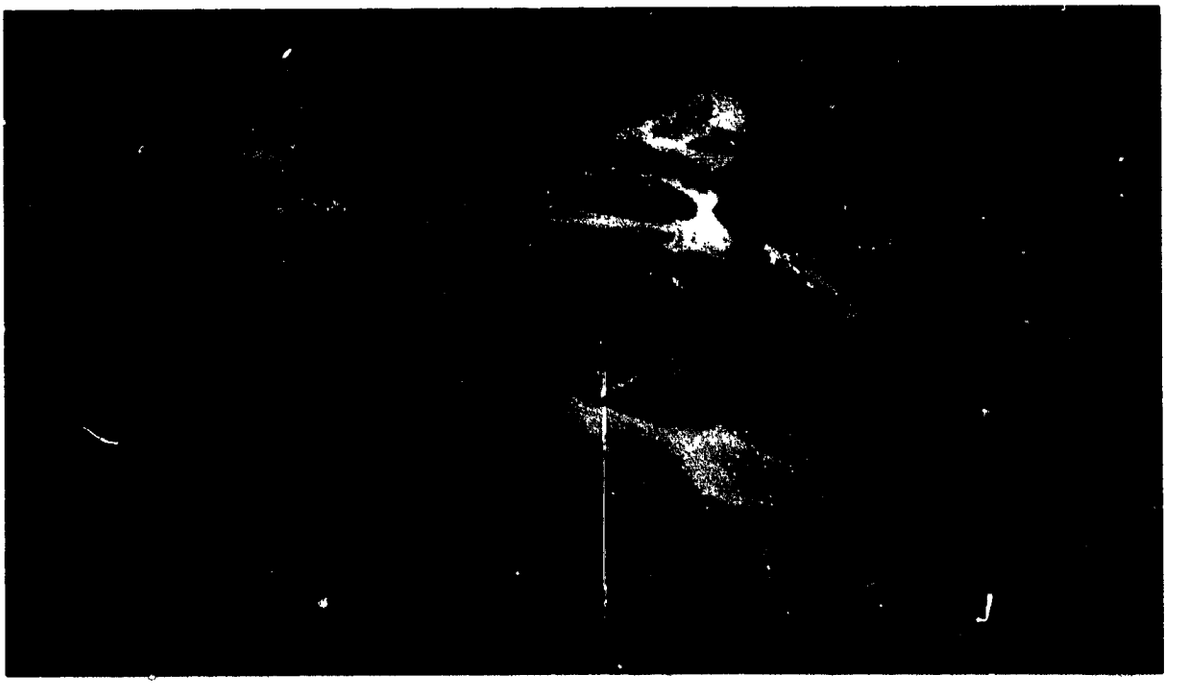

(a) M = 2.50.

L-83-76

Figure 5.- Oil flow photographs. Three jets operating; $\alpha = 20°$; $\beta = 0°$.

Jet off

$W_j/W_\infty = 0.0024$

(b) M = 3.50.

L-83-77

Figure 5.- Continued.

Jet off

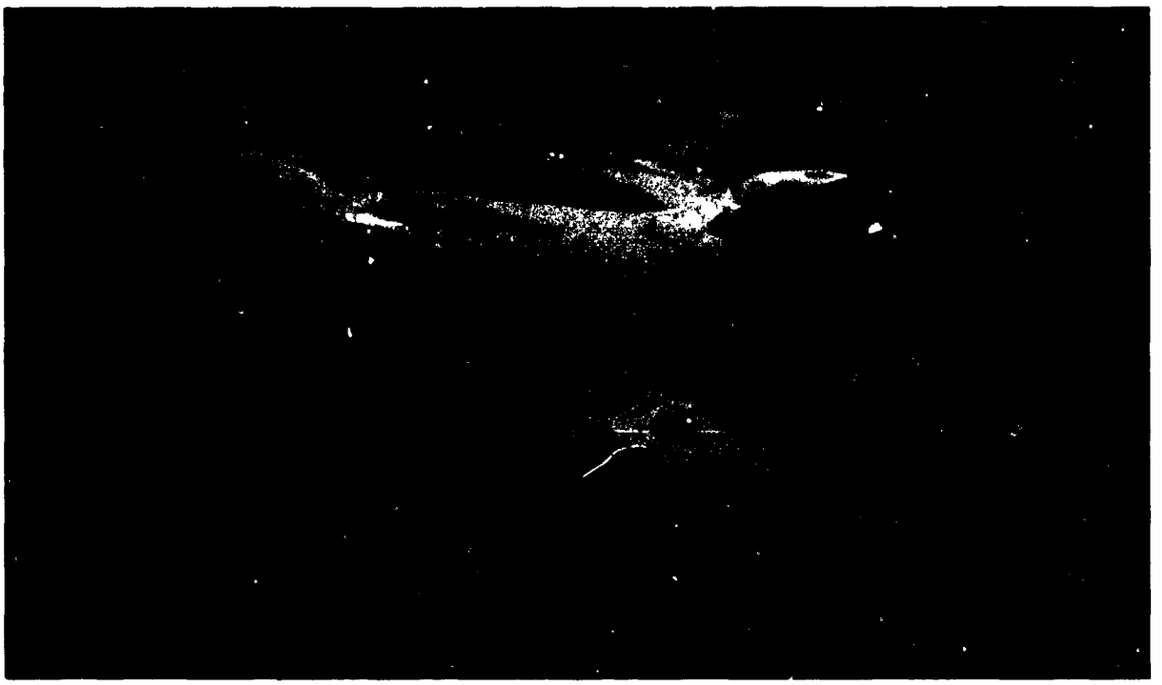

$W_j/W_\infty = 0.0024$

(c) M = 4.50.

L-83-78

Figure 5.- Concluded.

Jet off

$W_j/W_\infty = 0.0005$

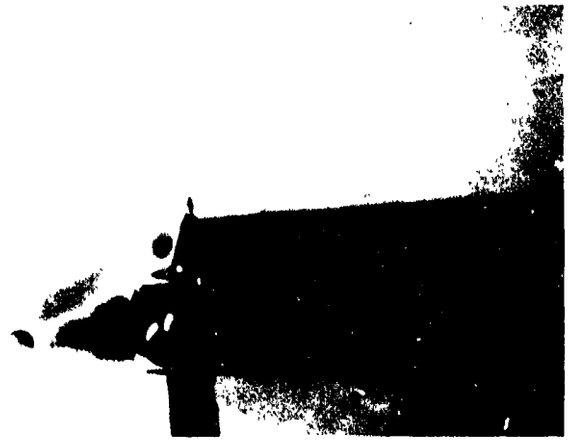

$W_j/W_\infty = 0.0024$

(a) M = 2.50; α = 20°.

L-83-79

Figure 6.- Vapor screen photographs. Light plane located at foremost jet orifice; β = 0°.

Jet off

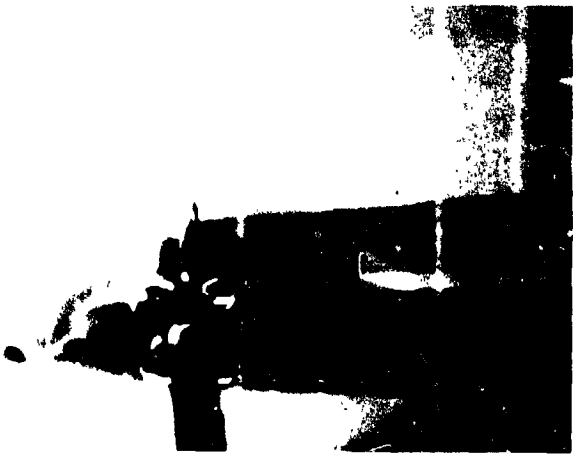

$W_j/W_\infty = 0.0024$

(b) M = 3.50; α = 20°.

L-83-80

Figure 6.- Continued.

Jet off

$W_j/W_\infty = 0.0005$

$W_j/W_\infty = 0.0024$

(c) M = 4.50; α = 20°.

L-83-81

Figure 6.- Concluded.

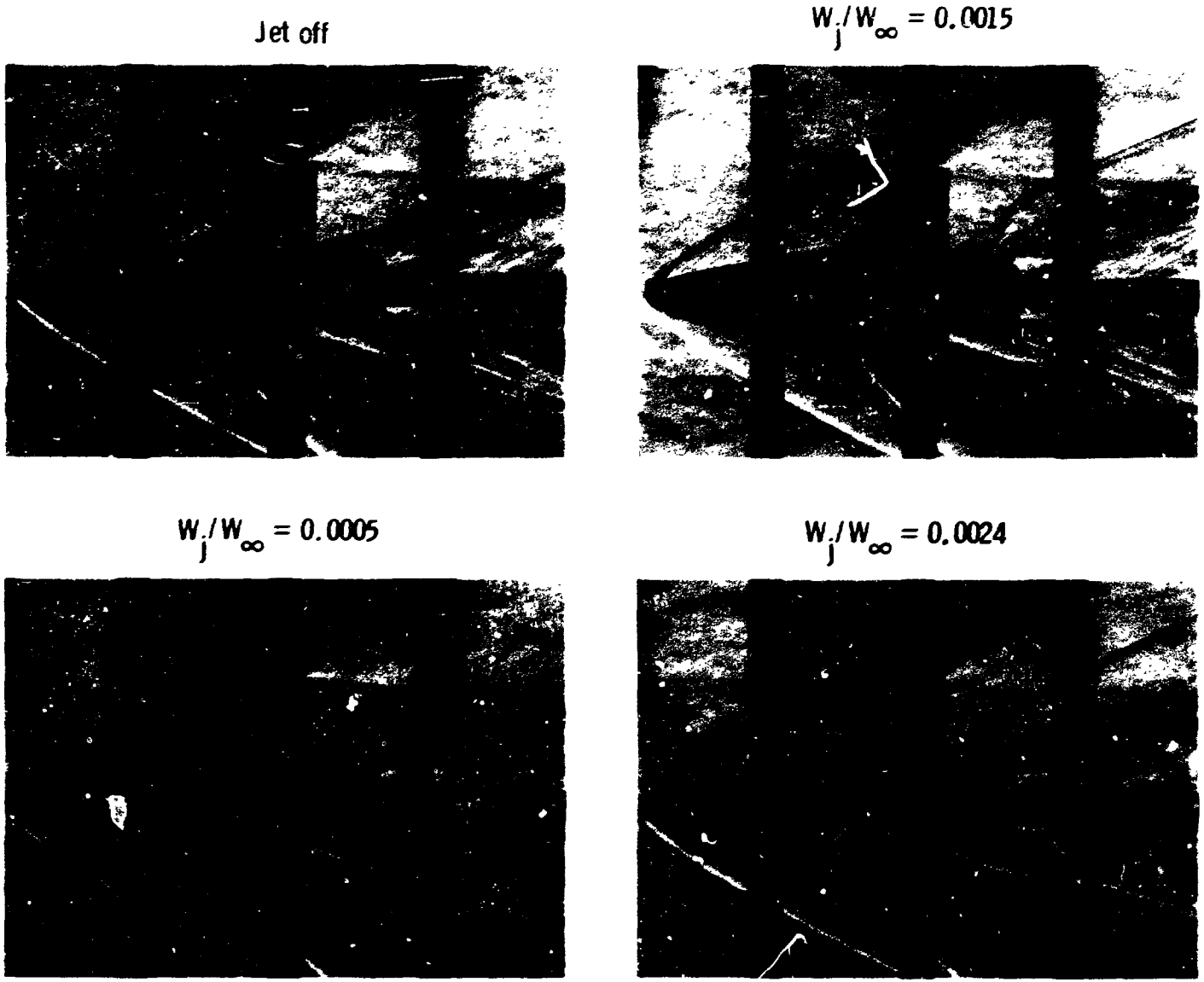

(a) M = 2.50; $\alpha = 20°$.

L-83-82

Figure 7.- Schlieren photographs. Elevons removed; three jets in operation; $\beta = 0°$.

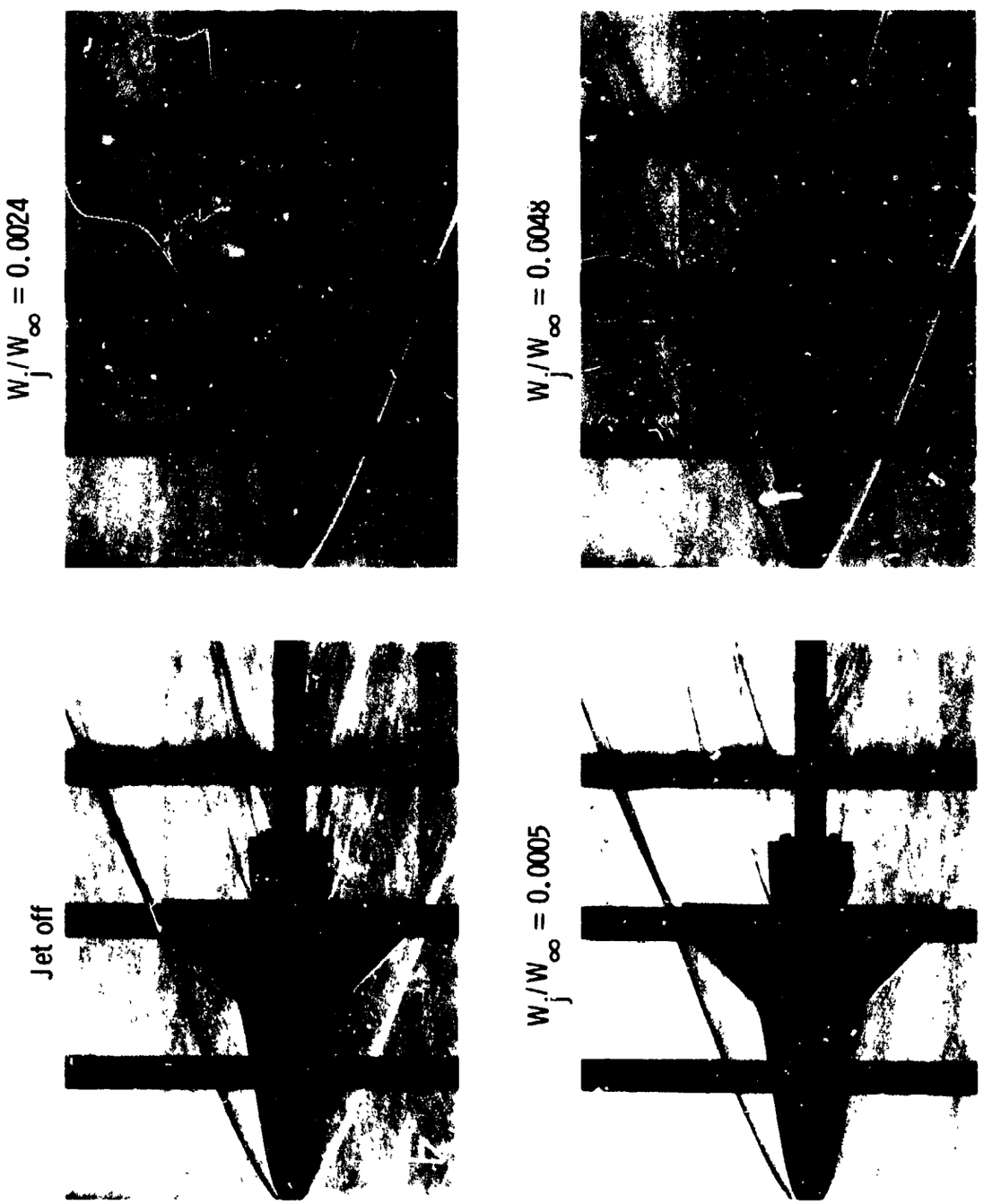

L-83-83

(b) M = 3.50; α = 17°.

Figure 7.- Continued.

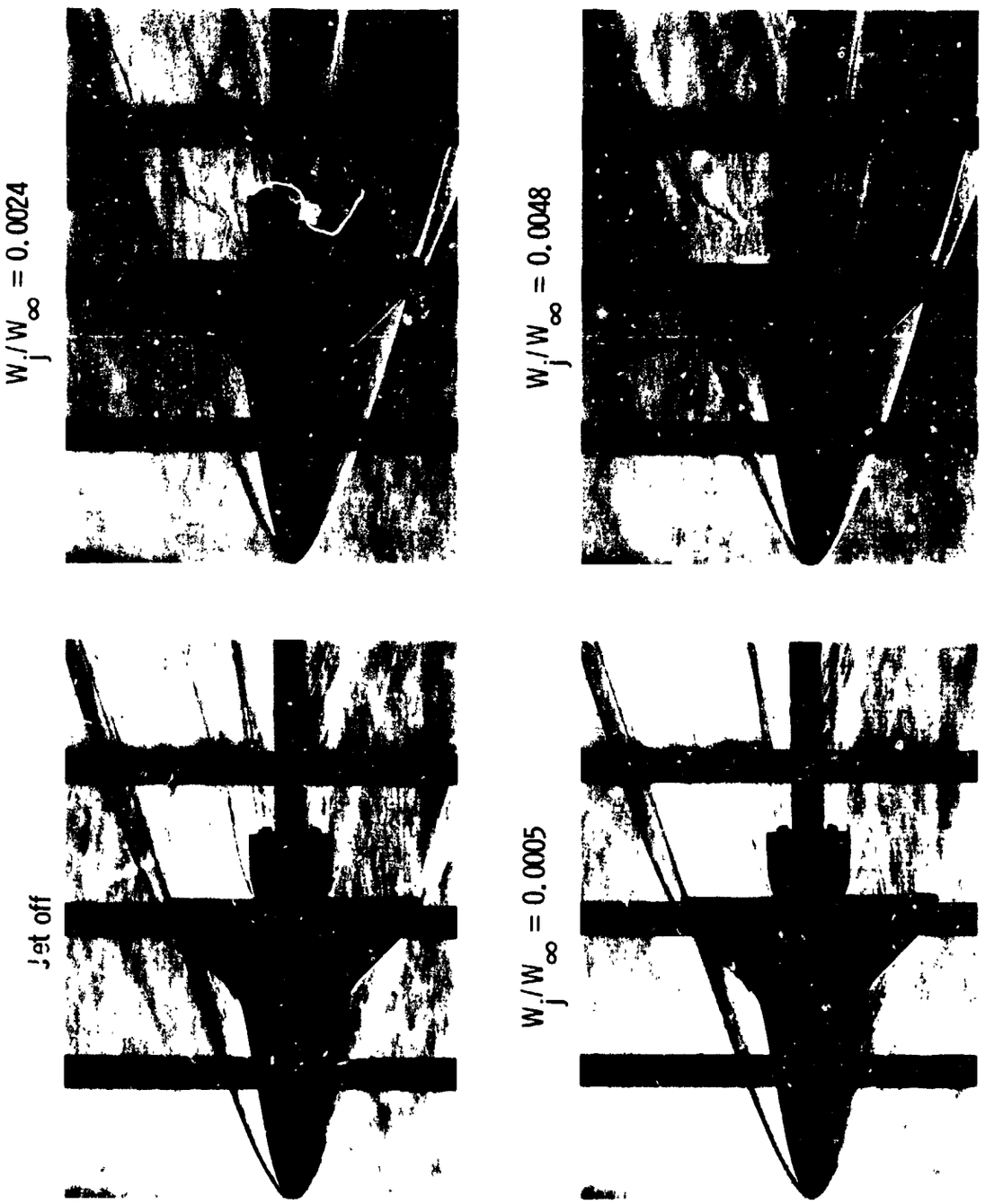

L-83-84

(c) M = 4.50; α = 20°.

Figure 7.- Concluded.

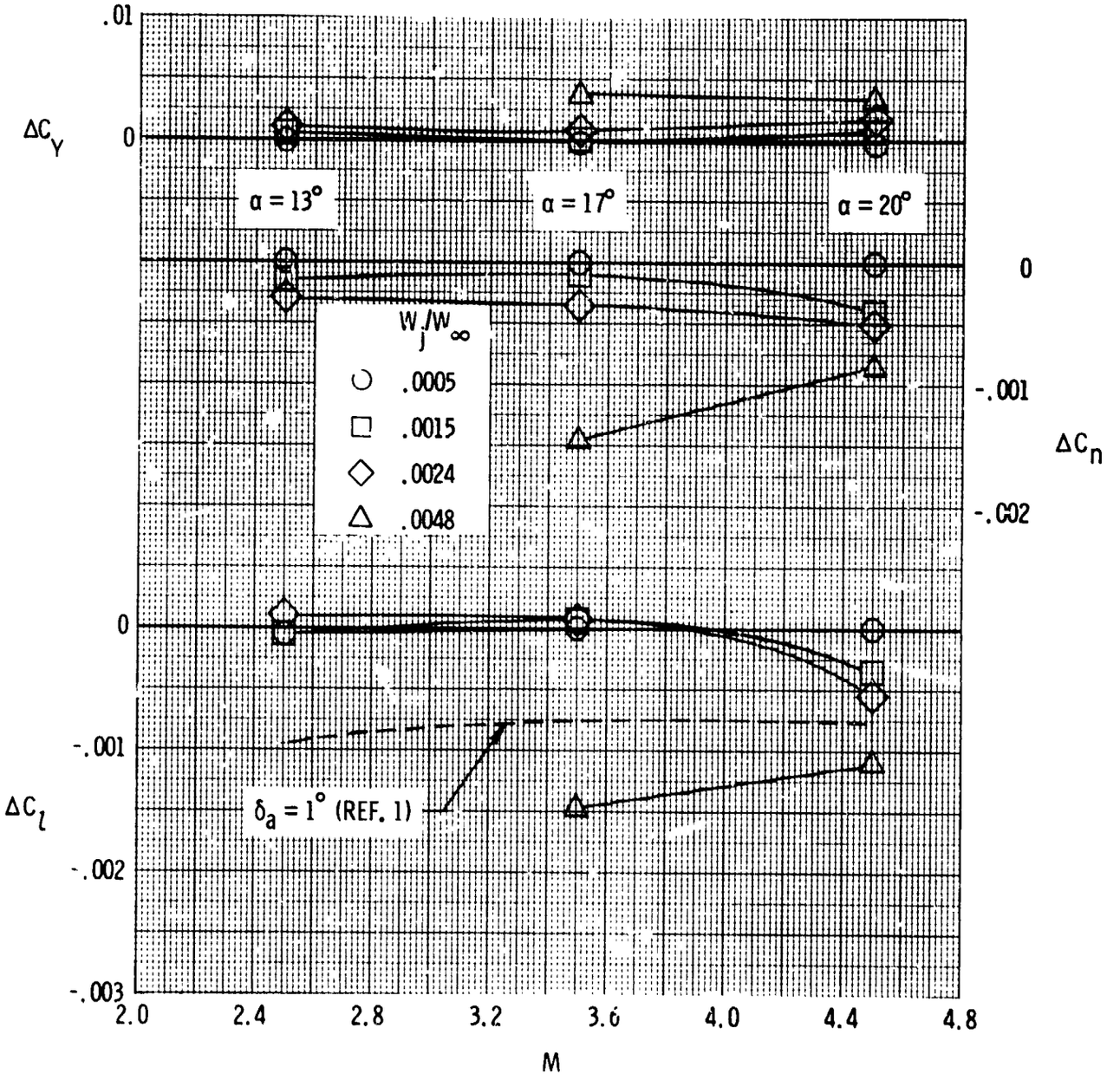

Figure 8.- Summary of incremental jet plume interference effects on lateral-directional aerodynamic characteristics at reentry angles of attack.

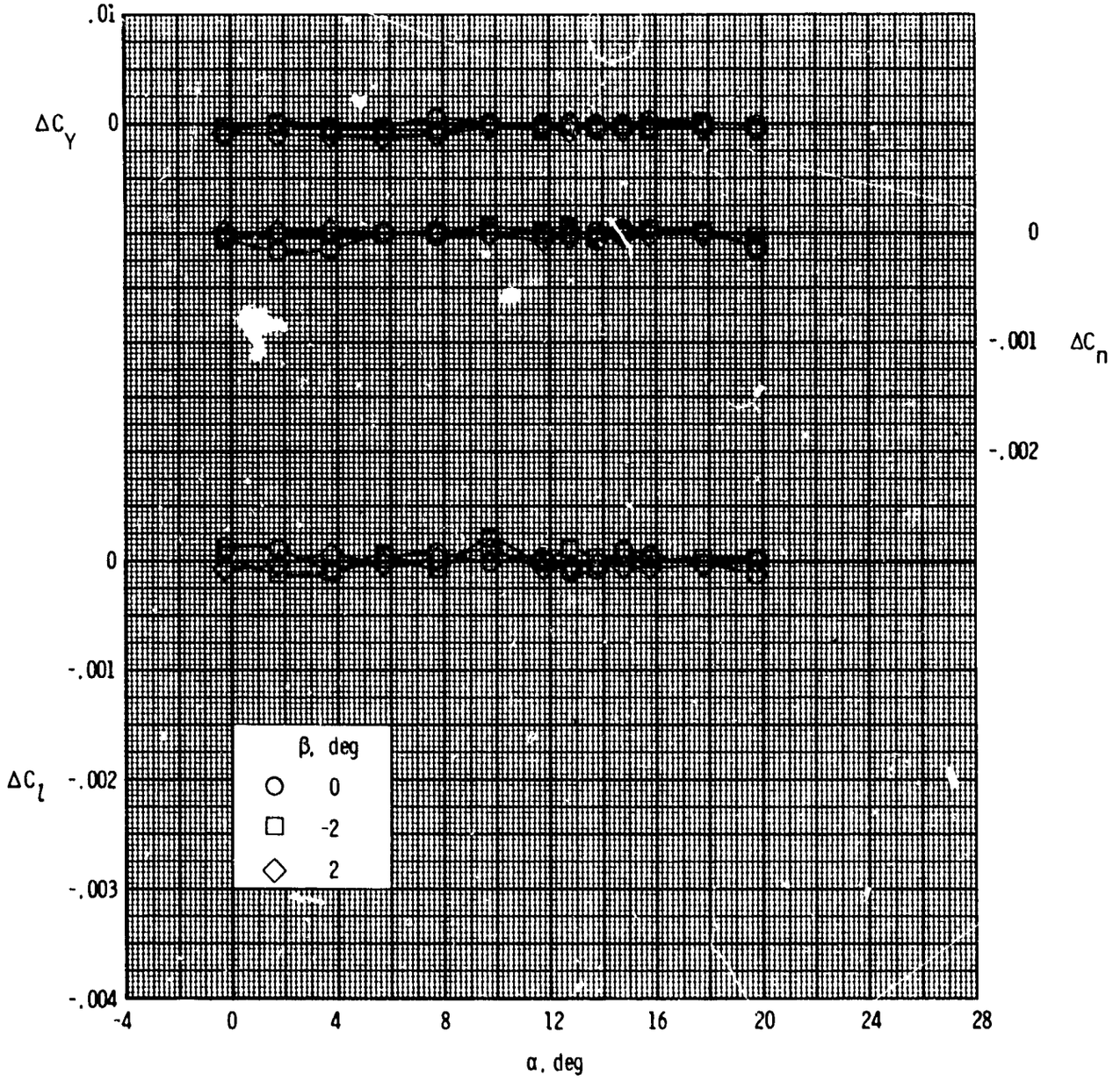

(a) M = 2.50; W_j/W_∞ = 0.0005.

Figure 9.- Effect of angle of sideslip on the jet interference increments. Three RCS yaw jets firing.

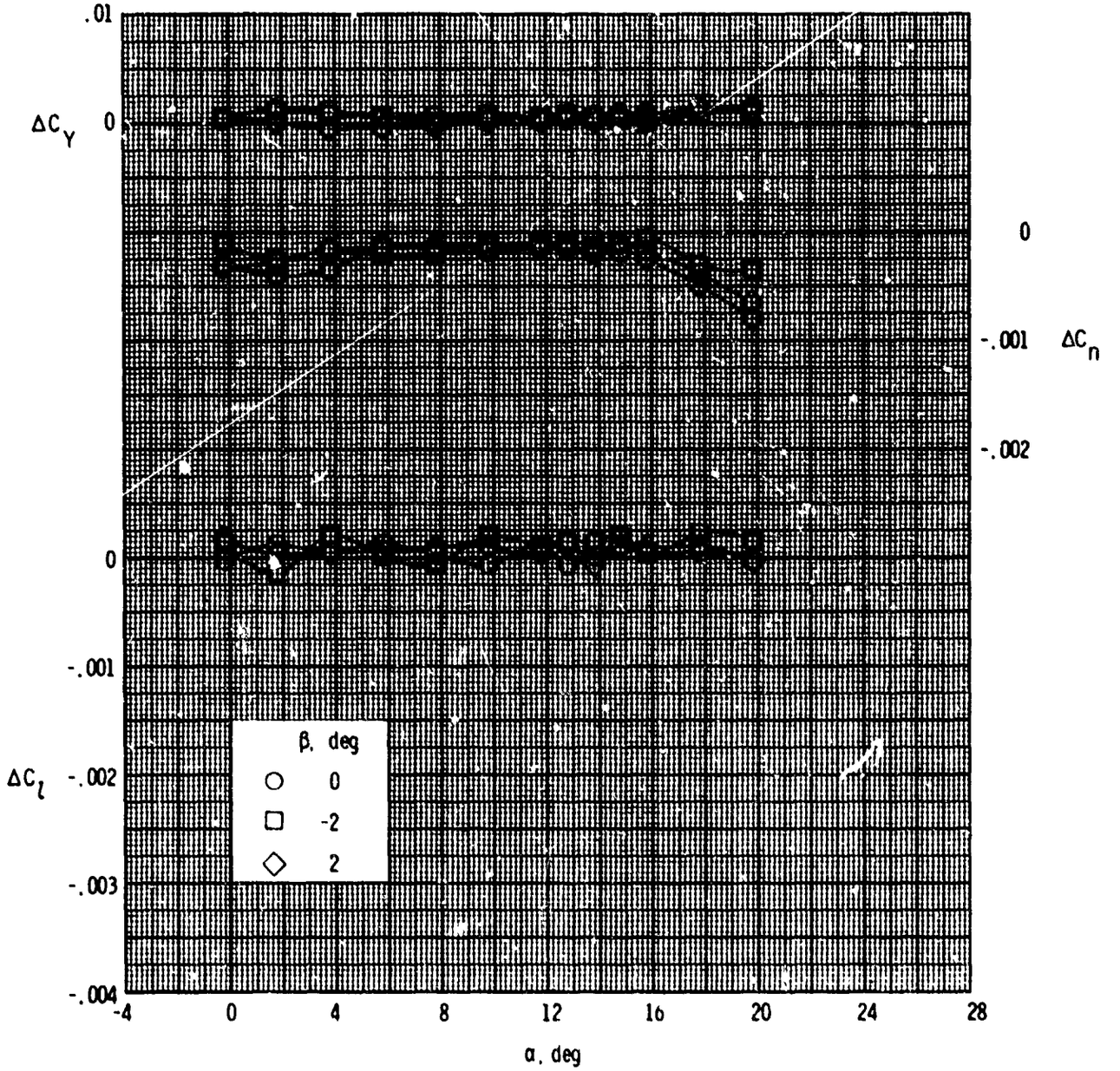

(b) $M = 2.50$; $W_j/W_\infty = 0.0015$.

Figure 9.- Continued.

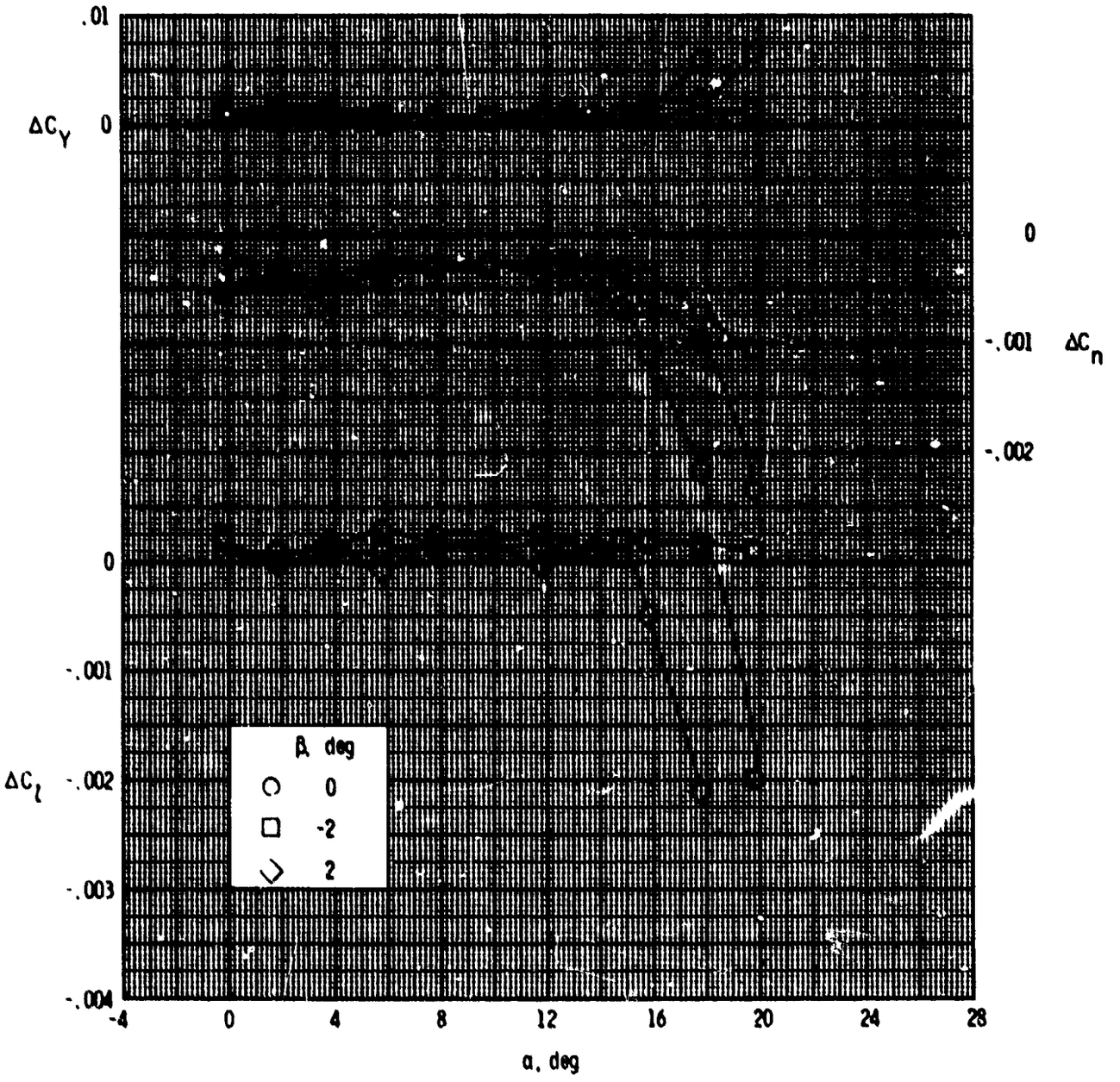

(c) M = 2.50; W_j/W_∞ = 0.0024.

Figure 9.- Continued.

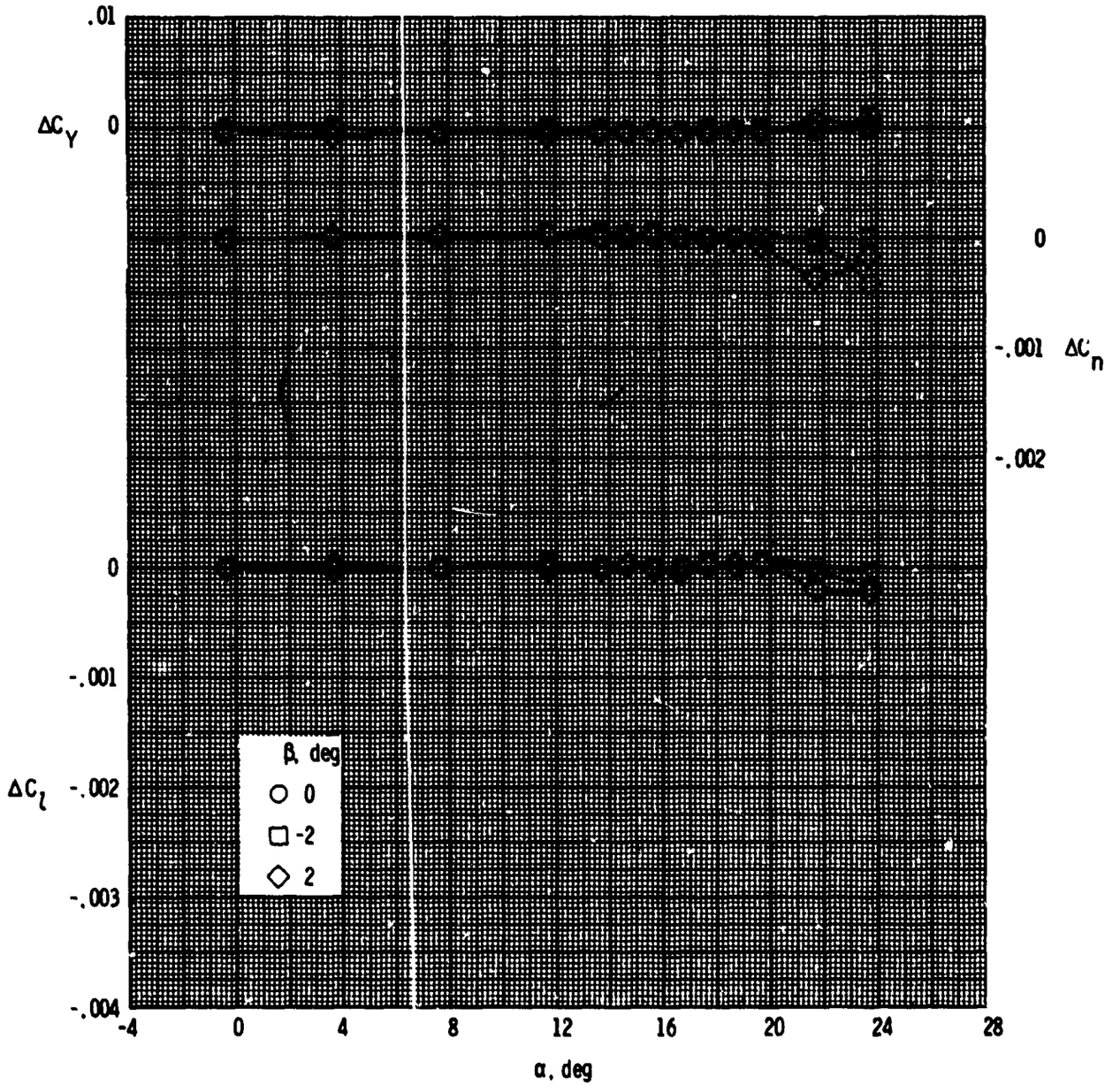

(d) M = 3.50; W_j/W_∞ = 0.0005.

Figure 9.- Continued.

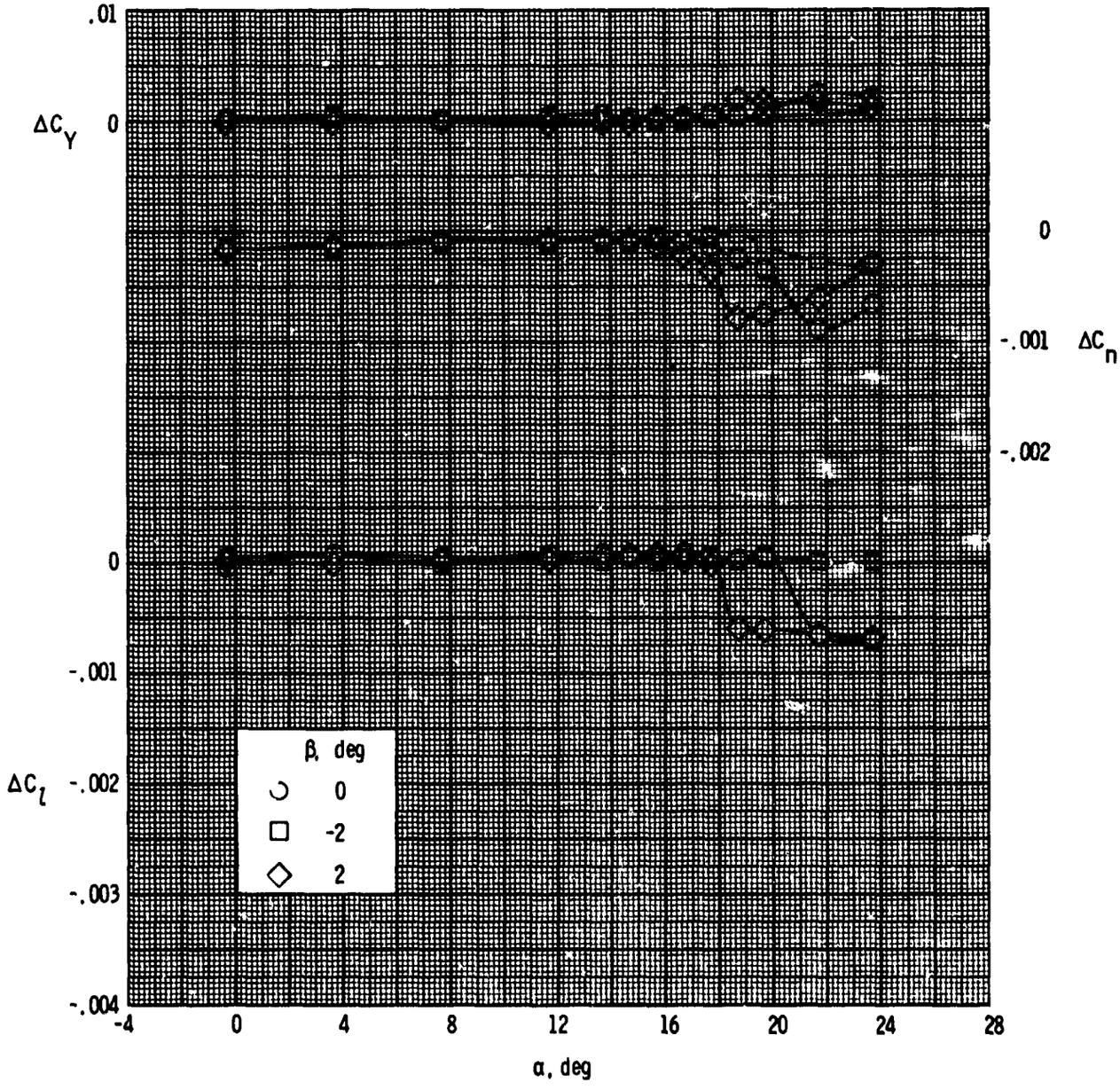

(e) M = 3.50; W_j/W_∞ = 0.0015.

Figure 9.- Continued.

ORIGINAL PAGE IS
OF POOR QUALITY

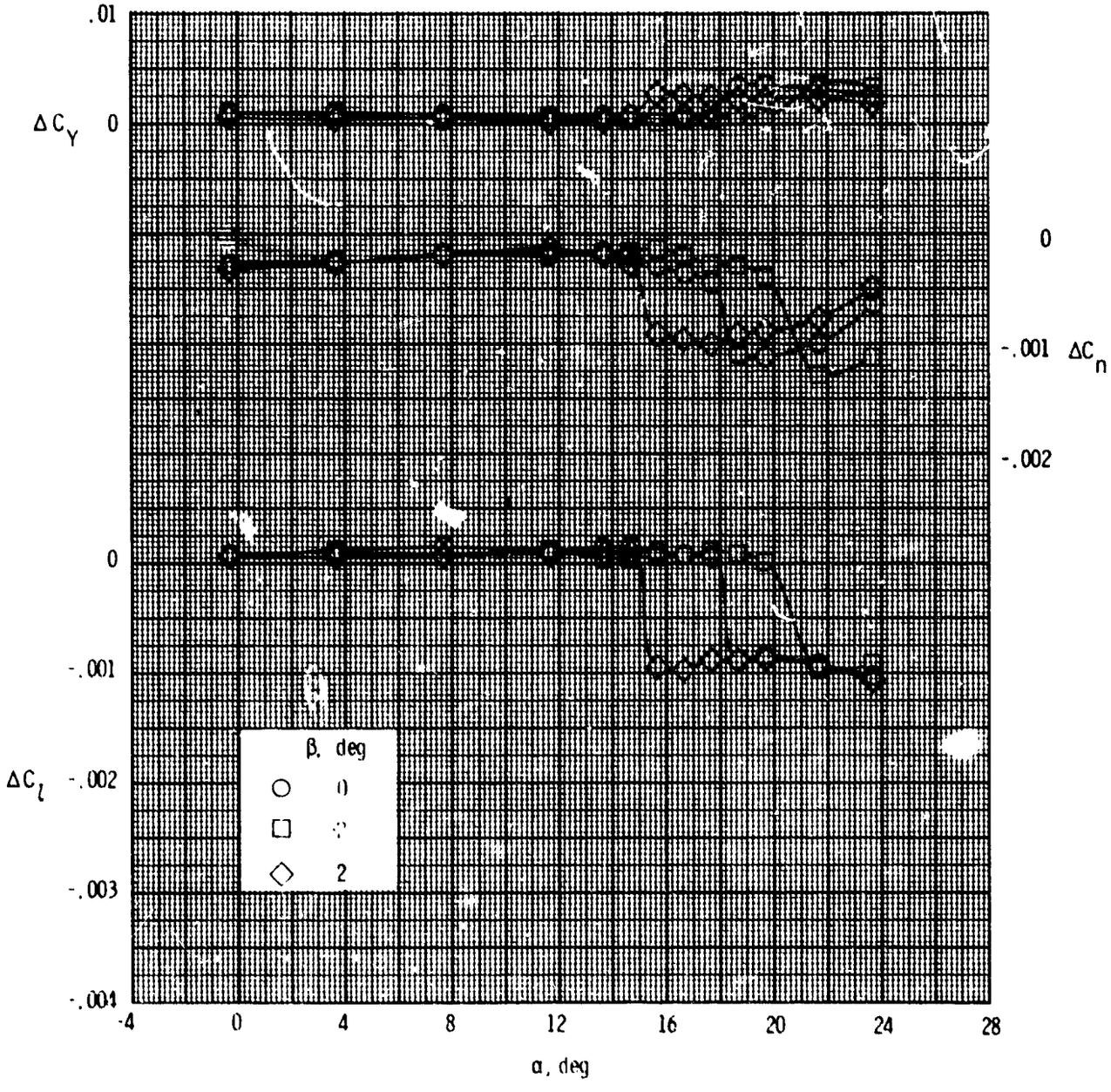

(t) M 3.50; W_1 W_∞ 0.0024.

Figure 9.- Continued.

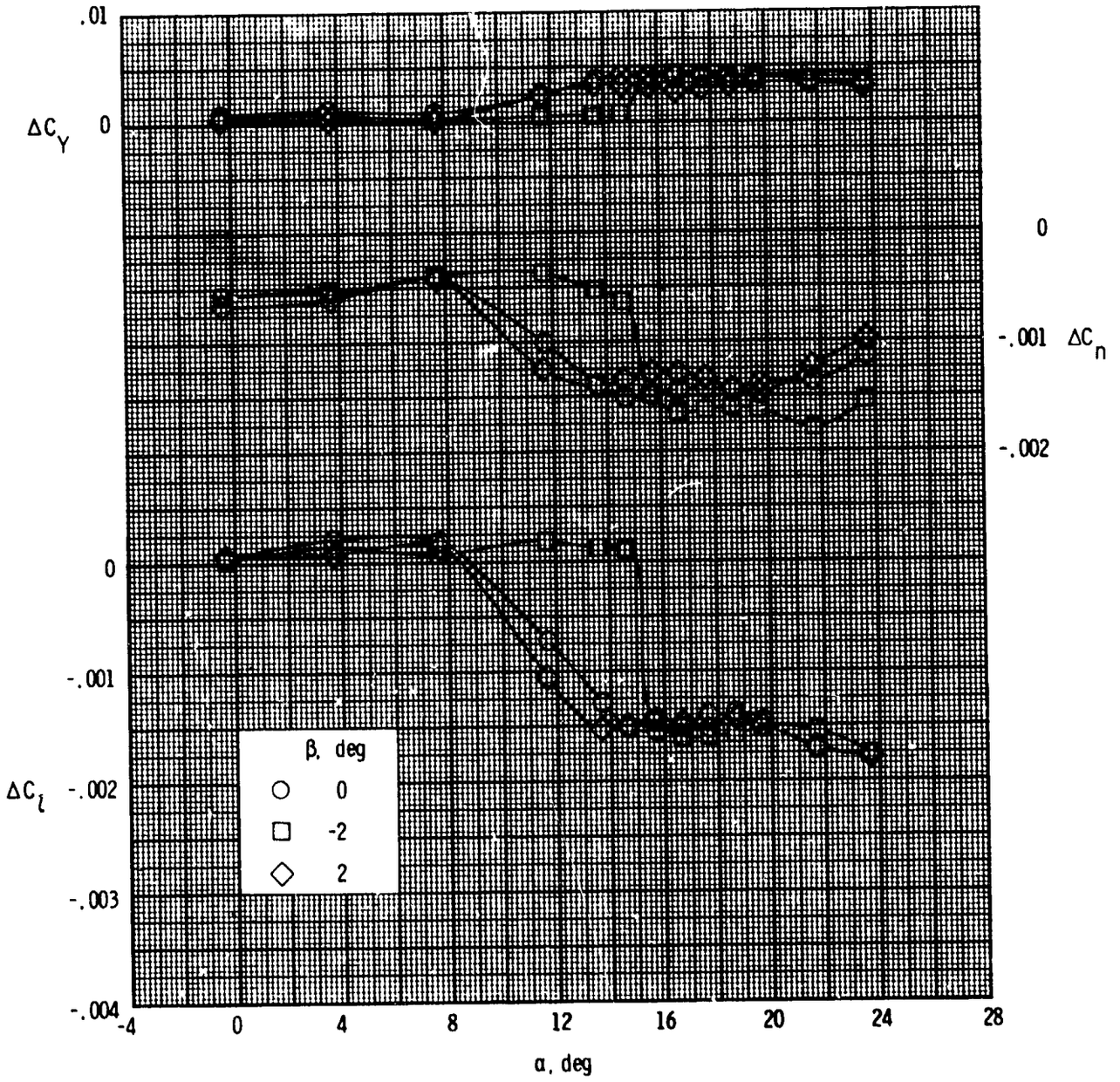

(q) M = 3.50; W_j/W_∞ = 0.0048.

Figure 9.- Continued.

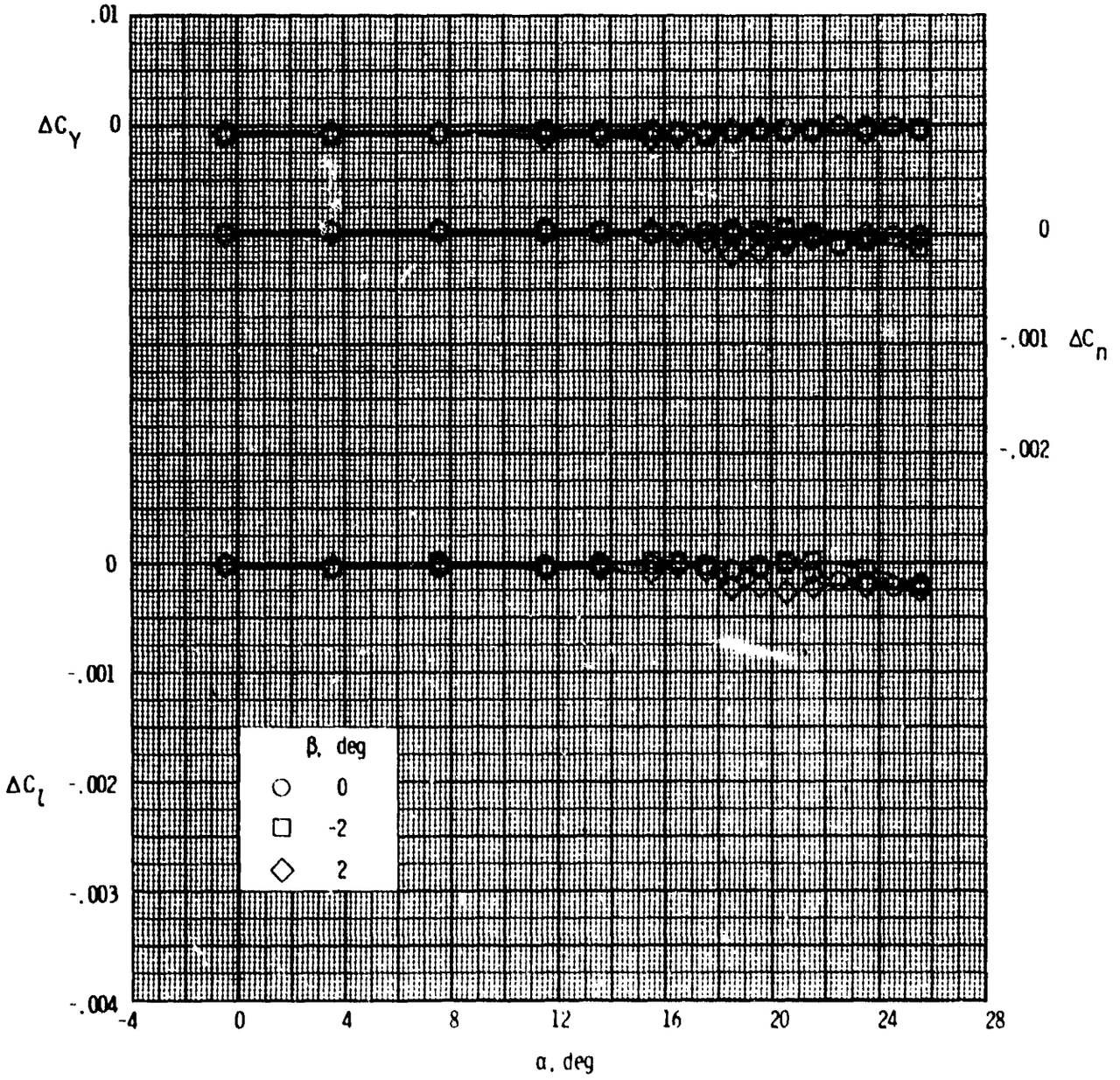

(h) M = 4.50; W_j/W_∞ = 0.0005.

Figure 9.- Continued.

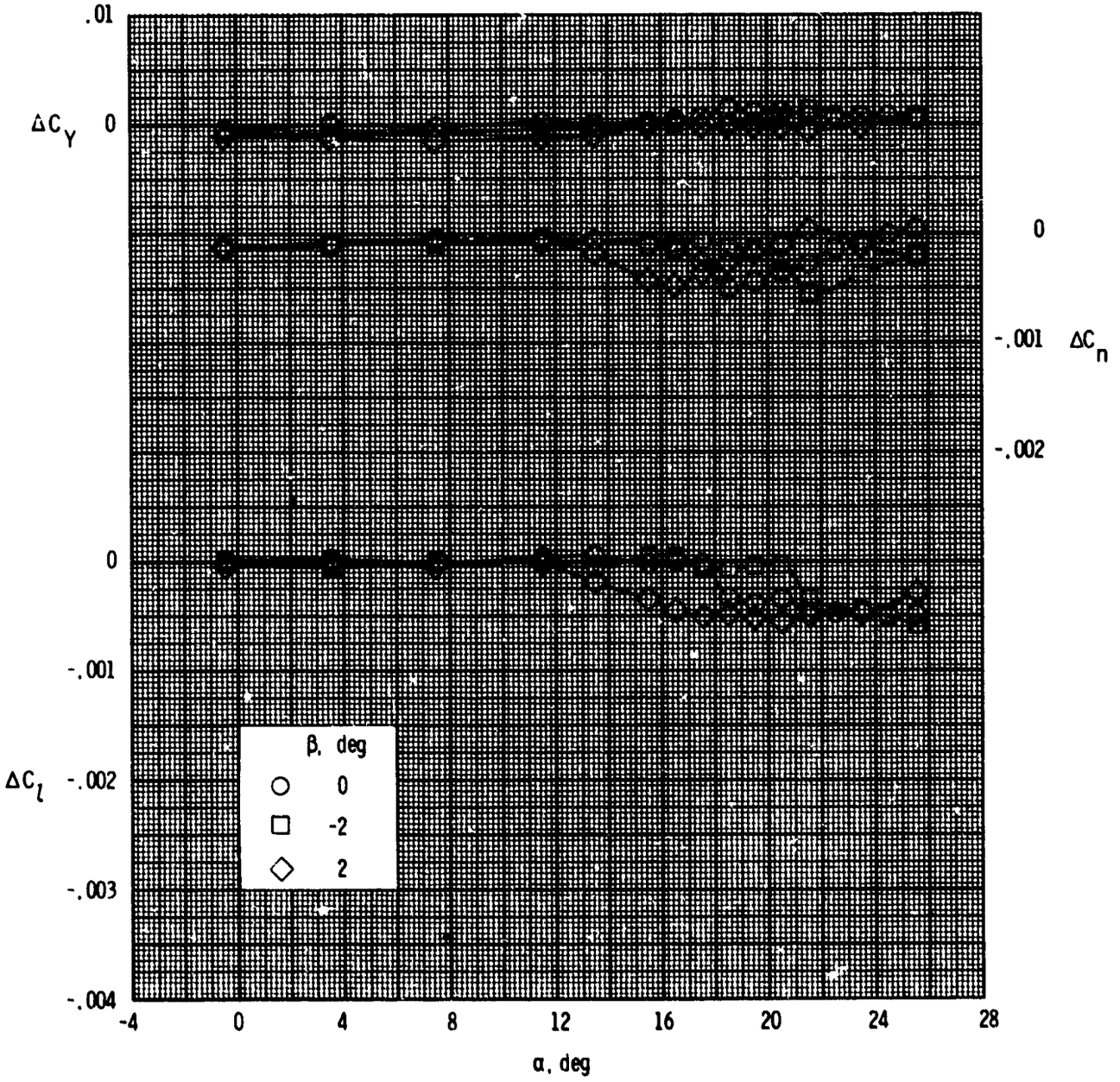

(i) M = 4.50; W_j/W_∞ = 0.0015.

Figure 9.- Continued.

ORIGINAL PAGE IS
OF POOR QUALITY

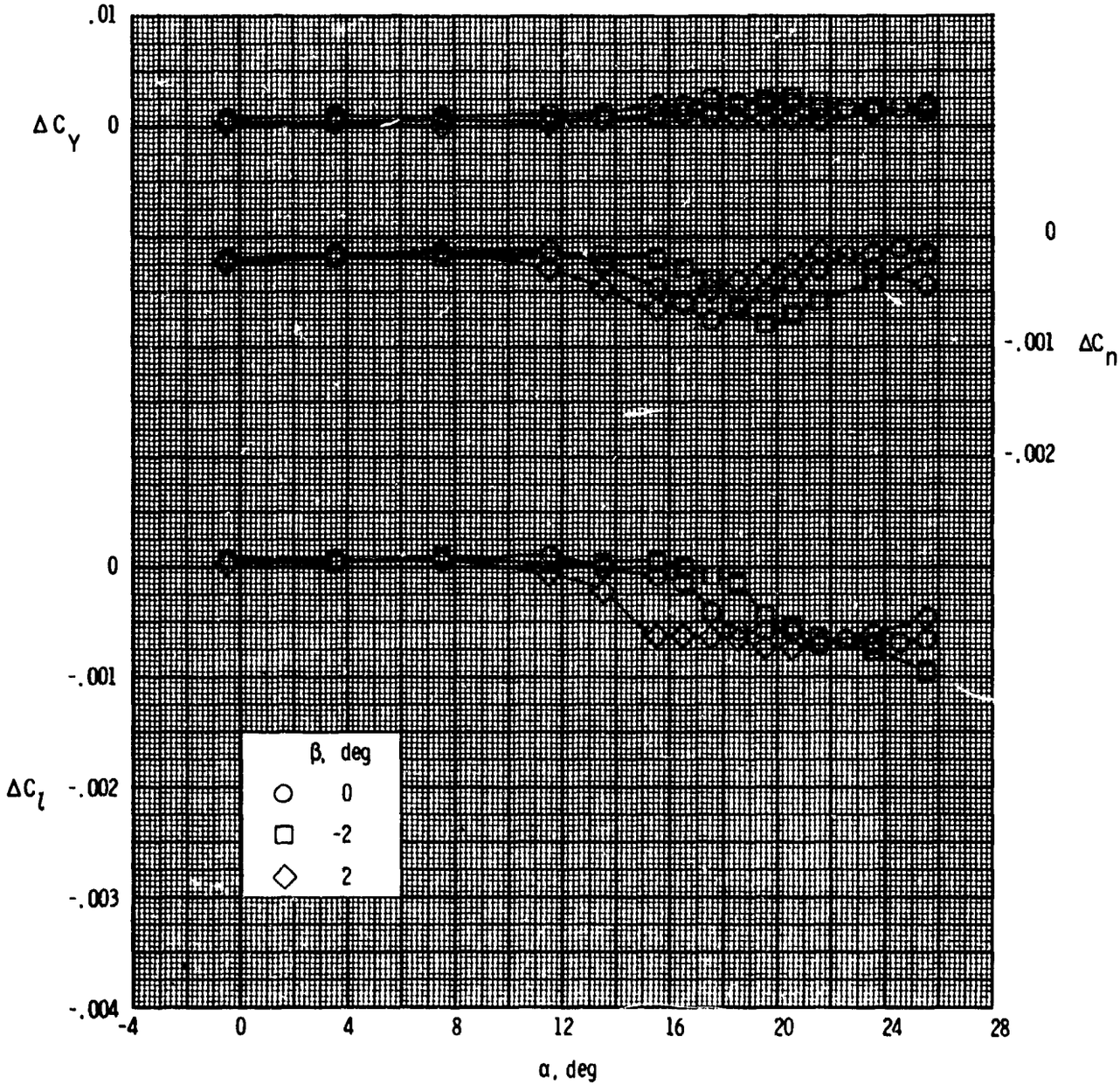

(j) M = 4.50; W_j/W_∞ = 0.0024.

Figure 9.- Continued.

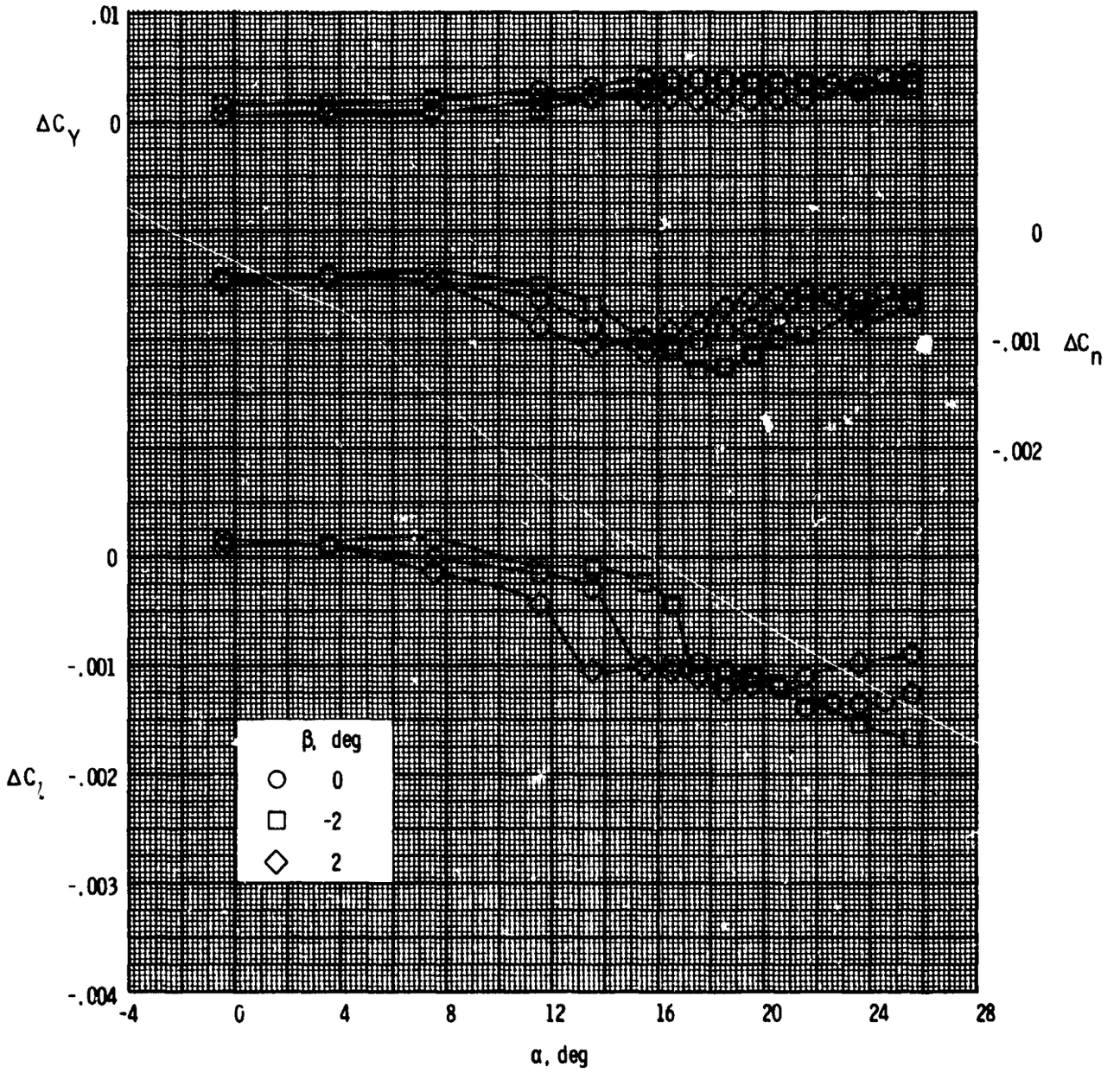

(k) M = 4.50; W_j/W_∞ = 0.0048.

Figure 9.- Continued.

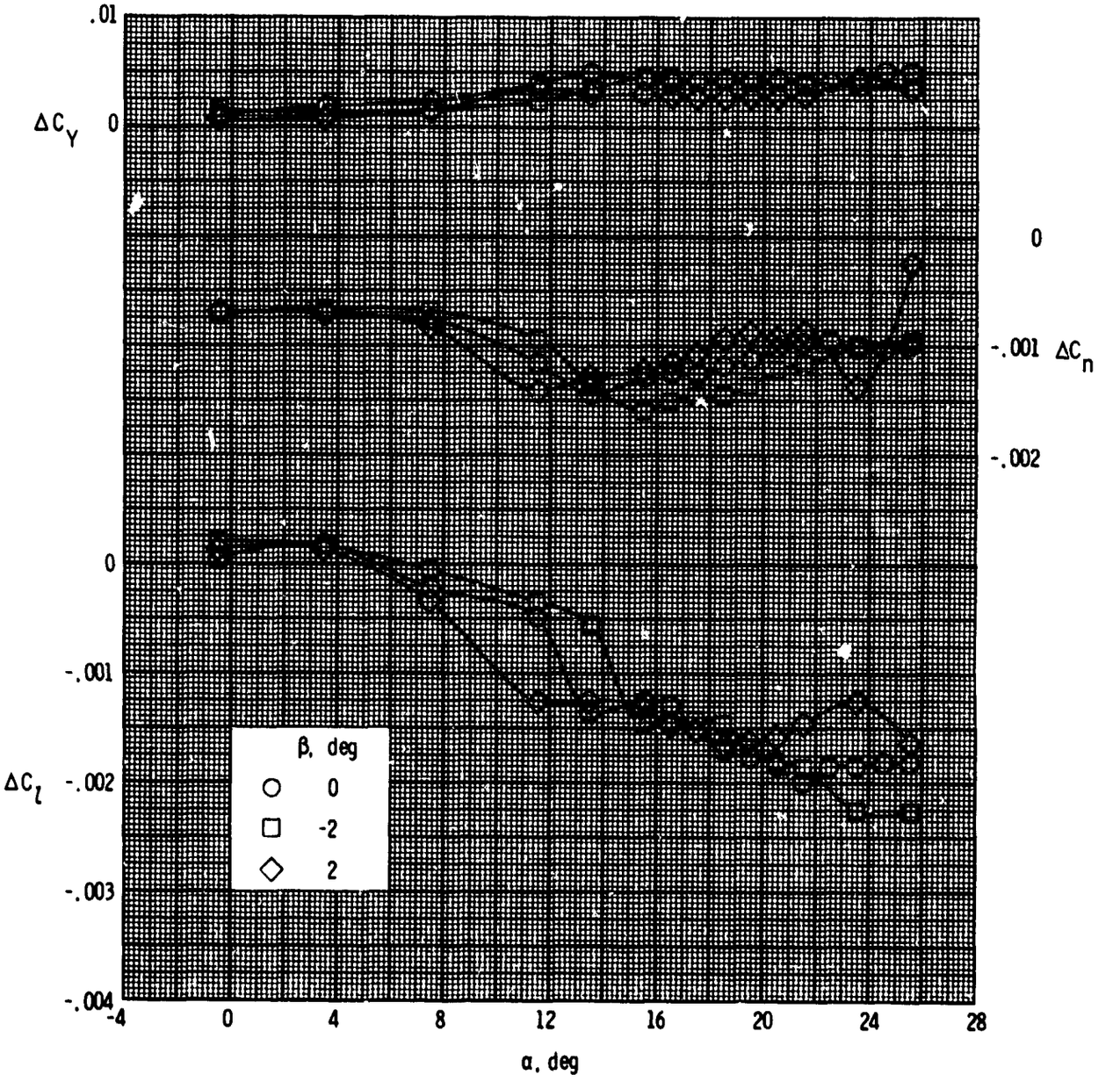

(1) M = 4.50; W_j/W_∞ = 0.0072.

Figure 9.- Concluded.

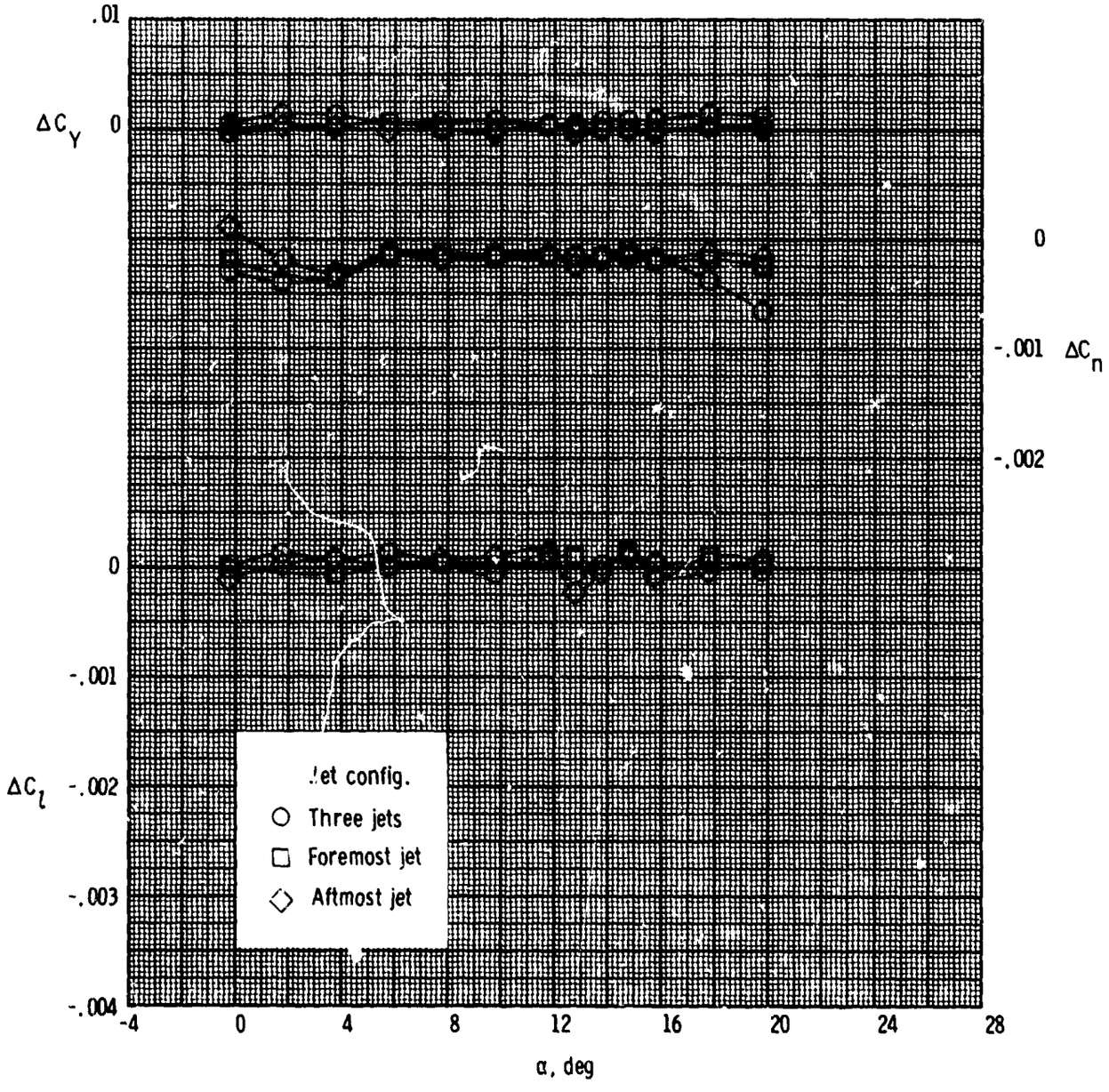

(a) M = 2.50.

Figure 10.- Effect of RCS yaw jet configuration on jet interference increments. W_j/W_∞ = 0.0014.

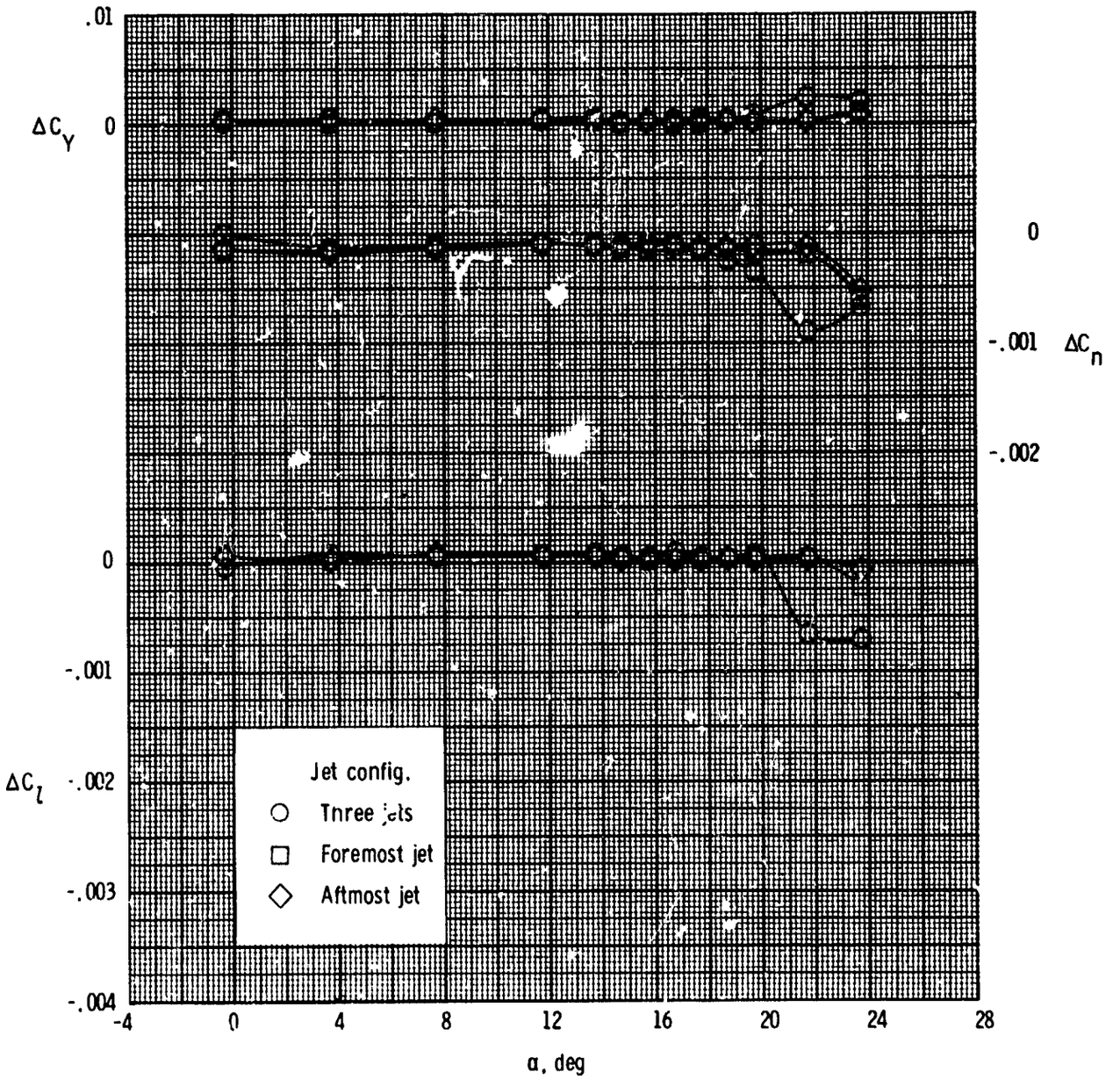

(b) M = 3.50.

Figure 10.- Continued.

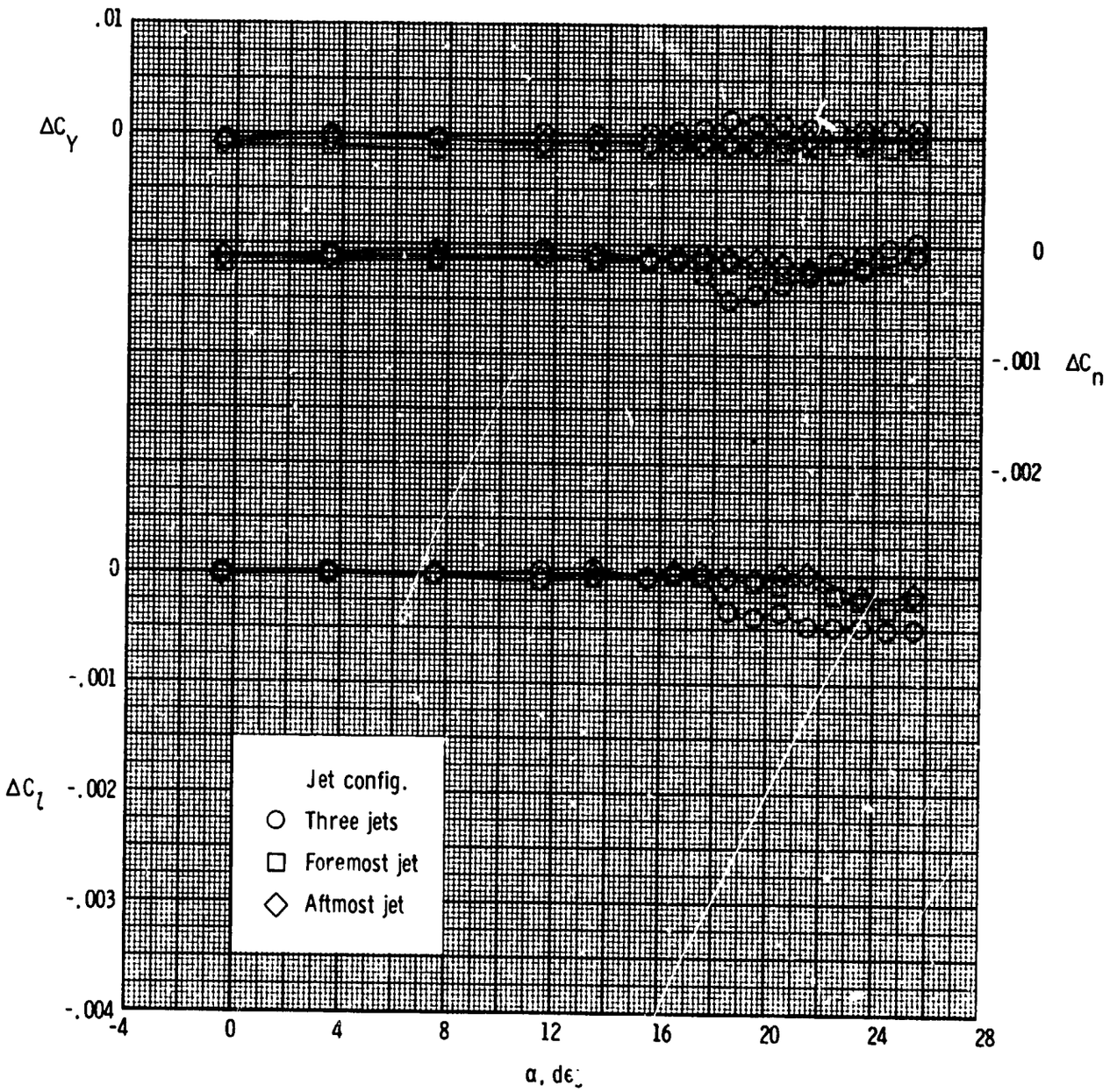

(c) M = 4.50.

Figure 10.- Concluded.

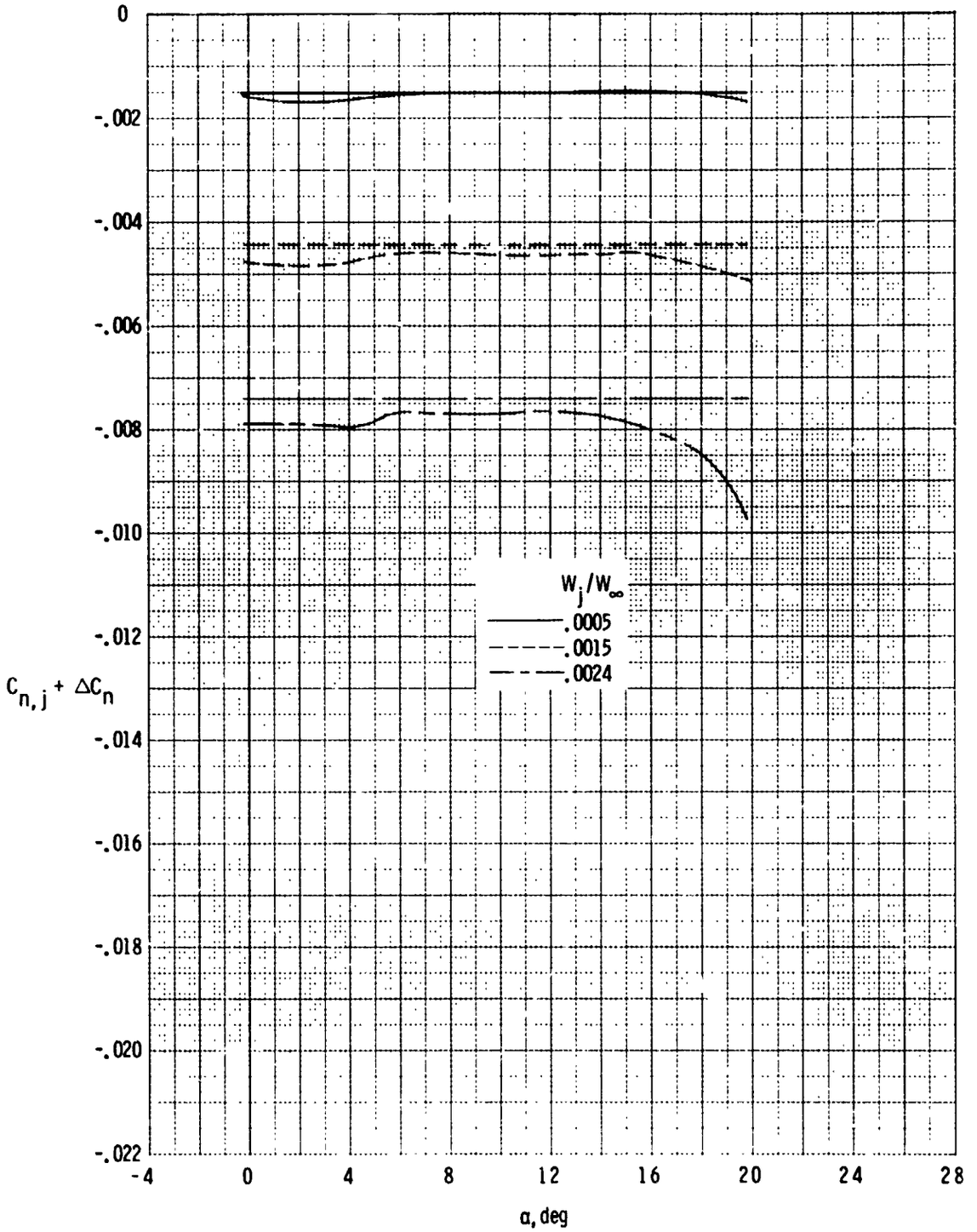

(a) M = 2.50.

Figure 11.- Yawing-moment coefficients due to jet thrust ($C_{n,j}$) and jet plume interference (ΔC_n). Straight horizontal line represents the jet thrust yawing-moment coefficient ($C_{n,j}$).

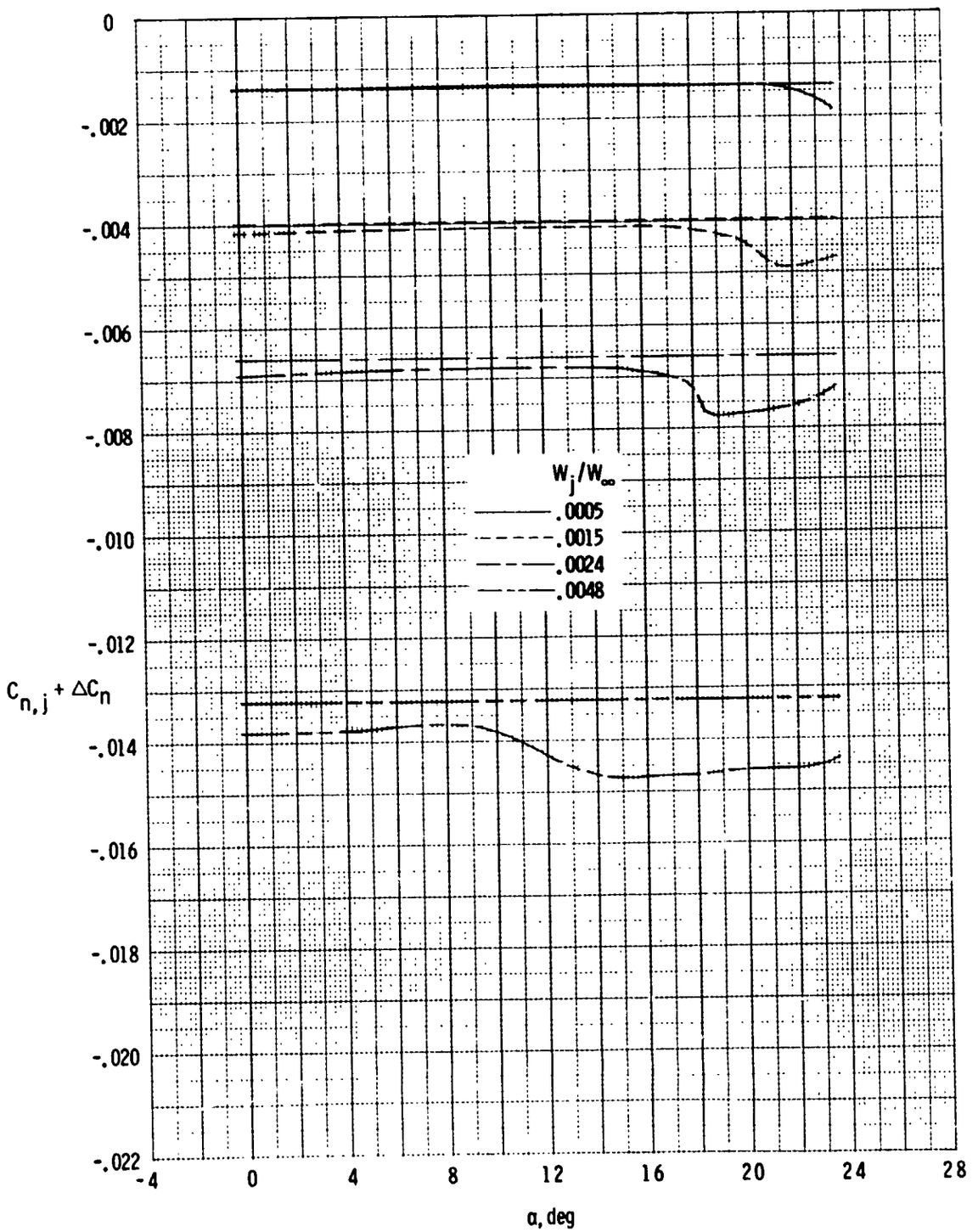

(b) M = 3.50.

Figure 11.- Continued.

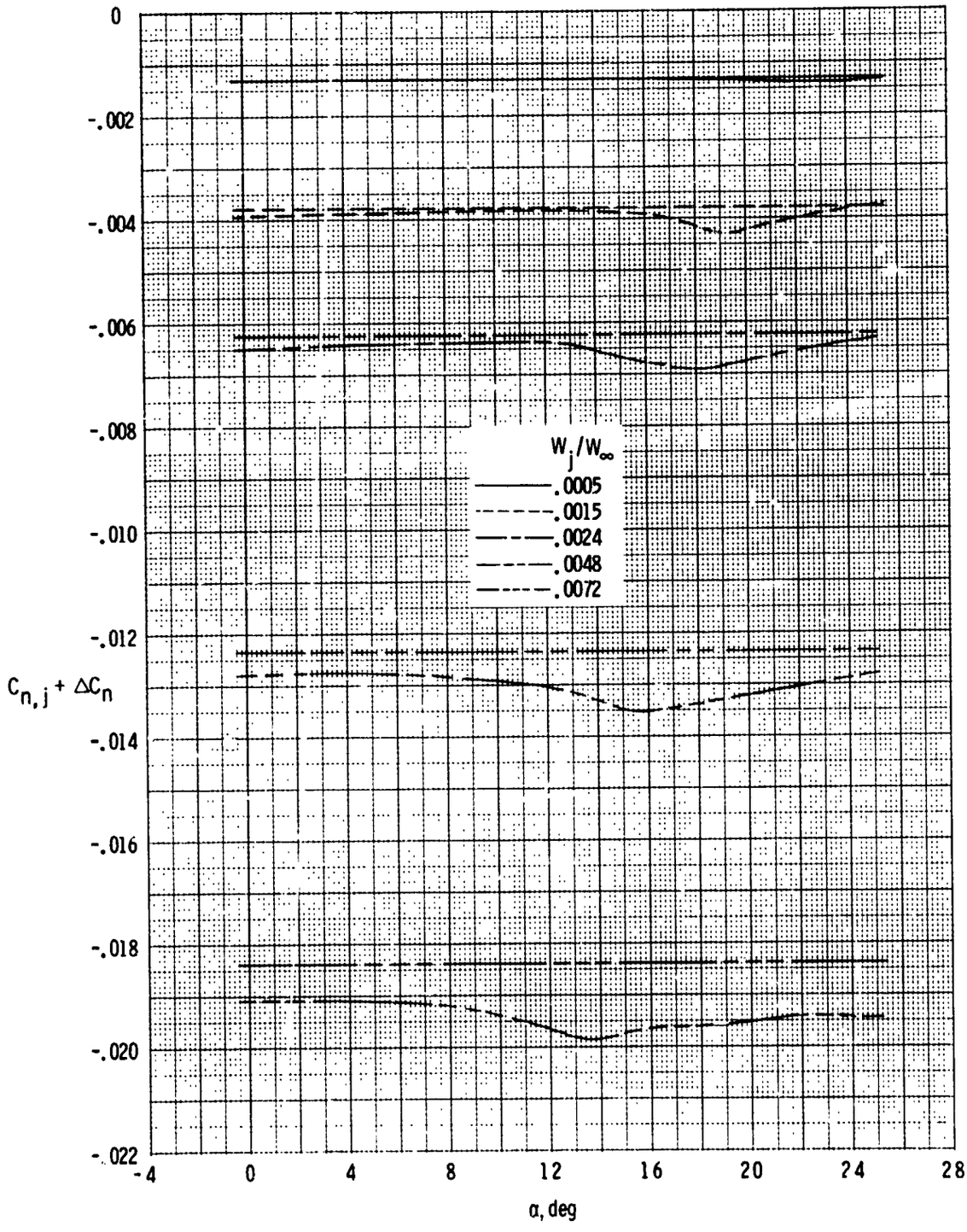

(c) M = 4.50.

Figure 11.- Concluded.